Galactic stellar haloes in the CDM model

A.P. Cooper[1]⋆, S. Cole[1], C.S. Frenk[1], S.D.M. White[2], J. Helly[1], A.J. Benson[3],
G. De Lucia[4], A. Helmi[5], A. Jenkins[1], J.F. Navarro[6], V. Springel[2], J. Wang[1]

[1]*Institute for Computational Cosmology, Department of Physics, University of Durham, South Road, Durham, DH1 3LE, UK*
[2]*Max-Planck-Institut für Astrophysik, Karl-Schwarzschild-Str. 1, D-85748, Garching, Germany*
[3]*Mail Code 350-17, California Institute of Technology, Pasadena, CA 91125, U.S.A.*
[4]*INAF-Osservatorio Astronomico di Trieste, Via G.B. Tiepolo 11, I-34131 Trieste, Italy*
[5]*Kapteyn Astronomical Institute, University of Groningen, P.O. Box 800, 9700 AV Groningen, Netherlands*
[6]*Department of Physics and Astronomy, University of Victoria, Victoria, BC V8P 5C2, Canada*

ABSTRACT

We present six simulations of Galactic stellar haloes formed by the tidal disruption of accreted dwarf galaxies in a fully cosmological setting. Our model is based on the Aquarius project, a suite of high resolution N-body simulations of individual dark matter haloes. We tag subsets of particles in these simulations with stellar populations predicted by the GAL-FORM semi-analytic model. Our method self-consistently tracks the dynamical evolution and disruption of satellites from high redshift. The luminosity function and structural properties of surviving satellites, which agree well with observations, suggest that this technique is appropriate. We find that accreted stellar haloes are assembled between $1 < z < 7$ from less than 5 significant progenitors. These progenitors are old, metal-rich satellites with stellar masses similar to the brightest Milky Way dwarf spheroidals ($10^7 - 10^8$ M$_\odot$). In contrast to previous stellar halo simulations, we find that several of these major contributors survive as self-bound systems to the present day. Both the number of these significant progenitors and their infall times are inherently stochastic. This results in great diversity among our stellar haloes, which amplifies small differences between the formation histories of their dark halo hosts. The masses ($\sim 10^8 - 10^9$ M$_\odot$) and density/surface-brightness profiles of the stellar haloes (from 10–100 kpc) are consistent with expectations from the Milky Way and M31. Each halo has a complex structure, consisting of well-mixed components, tidal streams, shells and other subcomponents. This structure is not adequately described by smooth models. The central regions (< 10 kpc) of our haloes are highly prolate ($c/a \sim 0.3$), although we find one example of a massive accreted thick disc. Metallicity gradients in our haloes are typically significant only where the halo is built from a small number of satellites. We contrast the ages and metallicities of halo stars with surviving satellites, finding broad agreement with recent observations.

Key words:
galaxies: haloes – galaxies: structure – galaxies: formation – galaxies: dwarf – Galaxy: halo – methods: *N*-body simulations – methods: numerical

1 INTRODUCTION

An extended and diffuse stellar halo envelops the Milky Way. Although only an extremely small fraction of the stars in the Solar neighbourhood belong to this halo, they can be easily recognized by their extreme kinematics and metallicities. Stellar populations with these properties can now be followed to distances in excess of 100 kpc using luminous tracers such as RR Lyraes, blue horizontal branch stars, metal-poor giants and globular clusters (e.g. Oort

1926; Baade 1944; Eggen, Lynden-Bell & Sandage 1962; Searle & Zinn 1978; Yanny et al. 2000; Vivas & Zinn 2006; Morrison et al. 2009).

In recent years, large samples of halo-star velocities (e.g. Morrison et al. 2000; Starkenburg et al. 2009) and 'tomographic' photometric and spectroscopic surveys have shown that the stellar halo is not a single smoothly-distributed entity, but instead a superposition of many components (Belokurov et al. 2006; Jurić et al. 2008; Bell et al. 2008; Carollo et al. 2007, 2009; Yanny et al. 2009). Notable substructures in the Milky Way halo include the broad stream of stars from the disrupting Sagittarius dwarf galaxy (Ibata, Gilmore

⋆ E-mail:a.p.cooper@durham.ac.uk

& Irwin 1994; Ibata et al. 2001), extensive and diffuse overdensities (Jurić et al. 2008; Belokurov et al. 2007a; Watkins et al. 2009), the Monoceros 'ring' (Newberg et al. 2002; Ibata et al. 2003; Yanny et al. 2003), the orphan stream (Belokurov et al. 2007b) and other kinematically cold debris (Schlaufman et al. 2009). Many of these features remain unclear. At least two kinematically distinct 'smooth' halo components have been identified from the motions of stars in the Solar neighbourhood, in addition to one or more 'thick disc' components (Carollo et al. 2009). Although current observations only hint at the gross properties of the halo and its substructures, some general properties are well-established: the halo is extensive ($> 100 \, \mathrm{kpc}$), metal-poor ($\langle [\mathrm{Fe/H}] \rangle \sim -1.6$, e.g. Laird et al. 1988; Carollo et al. 2009) and contains of the order of 0.1-1% of the total stellar mass of the Milky Way (recent reviews include Freeman & Bland-Hawthorn 2002; Helmi 2008).

Low surface-brightness features seen in projection around other galaxies aid in the interpretation of the Milky Way's stellar halo, and vice versa. Diffuse concentric 'shells' of stars on 100 kpc scales around otherwise regular elliptical galaxies have been attributed to accretion events (e.g. Schweizer 1980; Quinn 1984). Recent surveys of M31 (e.g. Ferguson et al. 2002; Kalirai et al. 2006; Ibata et al. 2007; McConnachie et al. 2009) have revealed an extensive halo (to $\sim 150 \, \mathrm{kpc}$) also displaying abundant substructure. The surroundings of other nearby Milky Way analogues are now being targeted by observations using resolved star counts to reach very low effective surface brightness limits, although as yet no systematic survey has been carried out to sufficient depth. (e.g. Zibetti & Ferguson 2004; McConnachie et al. 2006; de Jong, Radburn-Smith & Sick 2008; Barker et al. 2009; Ibata, Mouhcine, & Rejkuba 2009). A handful of deep observations beyond the Local Group suggest that stellar haloes are ubiquitous and diverse (e.g. Sackett et al. 1994; Shang et al. 1998; Malin & Hadley 1999; Martínez-Delgado et al. 2008, 2009; Faúndez-Abans et al. 2009).

Stellar haloes formed from the debris of disrupted satellites are a natural byproduct of hierarchical galaxy formation in the ΛCDM cosmology[1]. The entire assembly history of a galaxy may be encoded in the kinematics, metallicities, ages and spatial distributions of its halo stars. Even though these stars constitute a very small fraction of the total stellar mass, the prospects are good for recovering such information from the haloes of the Milky Way, M31 and even galaxies beyond the Local Group (e.g. Johnston, Hernquist & Bolte 1996; Helmi & White 1999). In this context, theoretical models can provide useful 'blueprints' for interpreting the great diversity of stellar haloes and their various sub-components, and for relating these components to fundamental properties of galaxy formation models. Alongside idealised models of tidal disruption, *ab initio* stellar halo simulations in realistic cosmological settings are essential for direct comparison with observational data.

In principle, hydrodynamical simulations are well-suited to this task, as they incorporate the dynamics of a baryonic component self-consistently. However, many uncertainties remain in how physical processes such as star formation and supernova feedback, which act below the scale of individual particles or cells, are implemented in these simulations. The computational cost of a sin-

gle state-of-the-art hydrodynamical simulation is extremely high. This cost severely limits the number of simulations that can be performed, restricting the freedom to explore different parameter choices or alternative assumptions within a particular model. The computational demands of hydrodynamical simulations are compounded in the case of stellar halo models, in which the stars of interest constitute only $\sim 1\%$ of the total stellar mass of a Milky Way-like galaxy. Even resolving the accreted dwarf satellites in which a significant proportion of these halo stars may originate is close to the limit of current simulations of disc galaxy formation. To date, few hydrodynamical simulations have focused explicitly on the accreted stellar halo (recent examples include Bekki & Chiba 2001; Brook et al. 2004; Abadi et al. 2006 and Zolotov et al. 2009).

In the wider context of simulating the 'universal' population of galaxies in representative ($\gtrsim 100 \, \mathrm{Mpc}^3$) cosmological volumes, these practical limitations of hydrodynamical simulations have motivated the development of a powerful and highly successful alternative, which combines two distinct modelling techniques: well-understood high-resolution N-body simulations of large-scale structure evolved self-consistently from ΛCDM initial conditions and fast, adaptable semi-analytic models of galaxy formation with very low computational cost per run (Kauffmann, Nusser & Steinmetz 1997; Kauffmann et al. 1999; Springel et al. 2001; Hatton et al. 2003; Kang et al. 2005; Springel et al. 2005; Bower et al. 2006; Croton et al. 2006; De Lucia et al. 2006). In this paper we describe a technique motivated by this approach which exploits computationally expensive, ultra-high-resolution N-body simulations of *individual* dark matter haloes by combining them with semi-analytic models of galaxy formation. Since our aim is to study the spatial and kinematic properties of stellar haloes formed through the tidal disruption of satellite galaxies, our technique goes beyond standard semi-analytic treatments.

The key feature of the method presented here is the dynamical association of stellar populations (predicted by the semi-analytic component of the model) with sets of *individual particles* in the N-body component. We will refer to this technique as 'particle tagging'. We show how it can be applied by combining the Aquarius suite of six high resolution isolated $\sim 10^{12} \, \mathrm{M_\odot}$ dark matter haloes (Springel et al. 2008a,b) with the GALFORM semi-analytic model (Cole et al. 1994, 2000; Bower et al. 2006). These simulations can resolve structures down to $\sim 10^6 \, \mathrm{M_\odot}$, comparable to the least massive dark halo hosts inferred for Milky Way satellites (e.g. Strigari et al. 2007; Walker et al. 2009).

Previous implementations of the particle-tagging approach (White & Springel 2000; Diemand, Madau & Moore 2005; Moore et al. 2006; Bullock & Johnston 2005; De Lucia & Helmi 2008) have so far relied on cosmological simulations severely limited by resolution (Diemand et al. 2005; De Lucia & Helmi 2008) or else simplified higher resolution N-body models (Bullock & Johnston 2005). In the present paper, we apply this technique as a postprocessing operation to a 'fully cosmological' simulation, in which structures have grown *ab initio*, interacting with one another self-consistently. The resolution of our simulations is sufficient to resolve stellar halo substructure in considerable detail.

With the aim of presenting our modelling approach and exploring some of the principal features of our simulated stellar haloes, we proceed as follows. In Section 2 we review the Aquarius simulations and their post-processing with the GALFORM model, and in Section 3 we describe our method for recovering the spatial distribution of stellar populations in the halo by tagging particles. We calibrate our model by comparing the statistical properties of the surviving satellite population to observations; the focus of

---

[1] In addition to forming components of the accreted stellar halo, infalling satellites may cause dynamical heating of a thin disc formed 'in situ' (e.g. Toth & Ostriker 1992; Velazquez & White 1999; Benson et al. 2004; Kazantzidis et al. 2008) and may also contribute material to an accreted thick disc (Abadi, Navarro & Steinmetz 2006) or central bulge. We discuss these additional contributions to the halo, some of which are not included in our modelling, in Section 3.3

this paper is on the stellar halo, rather on than the properties of these satellites. In Section 4 we describe our model stellar haloes and compare their structural properties to observations of the Milky Way and M31. We also examine the assembly history of the stellar haloes in detail (Section 4.2) and explore the relationship between the haloes and the surviving satellite population. Finally, we summarise our results in Section 5.

2 AQUARIUS AND GALFORM

Our model has two key components: the Aquarius suite of six high-resolution N-body simulations of Milky Way-like dark matter haloes, and GALFORM, a semi-analytic model of galaxy formation. The technique of post-processing an N-body simulation with a semi-analytic model is well established (Kauffmann et al. 1999; Springel et al. 2001; Helly et al. 2003; Hatton et al. 2003; Kang et al. 2005; Bower et al. 2006; De Lucia et al. 2006), although its application to high-resolution simulations of individual haloes such as Aquarius is novel and we review relevant aspects of the GALFORM code in this context below.

Here, in the post-processing of the N-body simulation, the stellar populations predicted by GALFORM to form in each halo are also associated with 'tagged' subsets of dark matter particles. By following these tagged dark matter particles, we track the evolving *spatial distribution and kinematics* of their associated stars, in particular those that are stripped from satellites to build the stellar halo. This level of detail regarding the distribution of halo stars is unavailable to a standard semi-analytic approach, in which the structure of each galaxy is represented by a combination of analytic density profiles.

Tagging particles in this way requires the fundamental assumption that baryonic mass nowhere dominates the potential and hence does not perturb the collisionless dynamics of the dark matter. Generally, a massive thin disc is expected to form at some point in the history of our 'main' haloes. Although our semi-analytic model accounts for this thin disc consistently, our dark matter tagging scheme cannot represent its dynamics. For this reason, and also to avoid confusion with our accreted halo stars, we do not attempt to tag dark matter to represent stars forming in situ in a thin disc at the centre of the main halo. The approximation that the dynamics of stars can be fairly represented by tagging dark matter particles is justifiable for systems with high mass-to-light ratios such as the dwarf satellites of the Milky Way and M31 (e.g. Simon & Geha 2007; Walker et al. 2009), the units from which stellar haloes are assembled in our models.

2.1 The Aquarius Haloes

Aquarius (Springel et al. 2008a) is a suite of high-resolution simulations of six dark matter haloes having masses within the range $1 - 2 \times 10^{12}$ M$_\odot$, comparable to values typically inferred for the Milky Way halo (e.g. Battaglia et al. 2005; Smith et al. 2007; Li & White 2008; Xue et al. 2008). By matching the abundance of dark matter haloes in the Millennium simulation to the SDSS stellar mass function, Guo et al. (2009) find 2.0×10^{12} M$_\odot$ (with a 10-90% range of 0.8×10^{12}M$_\odot$ to 4.7×10^{12}M$_\odot$). This value is sensitive to the assumption that the Milky Way is a typical galaxy, and to the adopted Milky Way stellar mass (5.5×10^{10} M$_\odot$; Flynn et al. 2006).

The Aquarius haloes were selected from a lower resolution version of the Millennium-II simulation (Boylan-Kolchin et al.

Table 1. Properties of the six Aquarius dark matter halo simulations (Springel et al. 2008a) on which the models in this paper are based. The first column labels the simulation (abbreviated from the as Aq-A-2, Aq-B-2 etc.). From left to right, the remaining columns give the particle mass $m_{\rm p}$, the number of particles within r_{200}, the virial radius at $z = 0$; the virial mass of the halo, M_{200}; and the maximum circular velocity, V_{max}, and corresponding radius, $r_{\max}$. Virial radii are defined as the radius of a sphere with mean inner density equal to 200 times the critical density for closure.

	$m_{\rm p}$ [10^3M$_\odot$]	N_{200} [10^6]	M_{200} [10^{12}M$_\odot$]	r_{200} [kpc]	$V_{\max}$ [km s^{-1}]	$r_{\max}$ [kpc]
A	13.70	135	1.84	246	209	28
B	6.447	127	0.82	188	158	40
C	13.99	127	1.77	243	222	33
D	13.97	127	1.74	243	203	54
E	9.593	124	1.19	212	179	56
F	6.776	167	1.14	209	169	43

2009) and individually resimulated using a multi-mass particle ('zoom') technique. In this paper we use the 'level 2' Aquarius simulations, the highest level at which all six haloes were simulated. We refer the reader to Springel et al. (2008a,b) for a comprehensive account of the entire simulation suite and demonstrations of numerical convergence. We list relevant properties of each halo/simulation in Table 1. The simulations were carried out with the parallel Tree-PM code GADGET-3, an updated version of GADGET-2 (Springel 2005). The Aq-2 simulations used a fixed comoving Plummer-equivalent gravitational softening length of $\epsilon = 48 \ h^{-1}$ pc. ΛCDM cosmological parameters were adopted as $\Omega_{\rm m} = 0.25$, $\Omega_\Lambda = 0.75$, $\sigma_8 = 0.9$, $n_{\rm s} = 1$, and Hubble constant $H_0 = 100h$ km s^{-1}Mpc^{-1}. A value of $h = 0.73$ is assumed throughout this paper. These parameters are identical to those used in the Millennium Simulation and are marginally consistent with WMAP 1- and 5-year constraints (Spergel et al. 2003; Komatsu et al. 2009).

2.2 The GALFORM Model

N-body simulations of cosmic structure formation supply information on the growth of dark matter haloes, which can serve as the starting point for a semi-analytic treatment of baryon accretion, cooling and star formation (see Baugh 2006, for a comprehensive discussion of the fundamental principles of semi-analytic modelling). The Durham semi-analytic model, GALFORM, is used in this paper to postprocess the Aquarius N-body simulations. The GALFORM code is controlled by a number of interdependent parameters which are constrained in part by theoretical limits and results from hydrodynamical simulations. Remaining parameter values are chosen such that the model satisfies statistical comparisons with several datasets, for example the galaxy luminosity function measured in several wavebands (e.g. Baugh et al. 2005; Bower et al. 2006; Font et al. 2008). Such statistical constraints on large scales do not guarantee that the same model will provide a good description of the evolution of a single 'Milky Way' halo and its satellites. A model producing a satellite galaxy luminosity function consistent with observations is a fundamental prerequisite for the work presented here, in which a proportion of the total satellite population provides the raw material for the assembly of stellar haloes. We demonstrate below that the key processes driving galaxy formation

on small scales are captured to good approximation by the existing GALFORM model and parameter values of Bower et al. (2006).

Many of the physical processes of greatest relevance to galaxy formation on small scales were explored within the context of semi-analytic modelling by Benson et al. (2002b). Of particular significance are the suppression of baryon accretion and cooling in low mass haloes as the result of photoheating by a cosmic ionizing background, and the effect of supernova feedback in shallow potential wells. Together, these effects constitute a straightforward astrophysical explanation for the disparity between the number of low mass dark subhaloes found in N-body simulations of Milky Way-mass hosts and the far smaller number of luminous satellites observed around the Milky Way (the so-called 'missing satellite' problem). Recent discoveries of faint dwarf satellites and an improved understanding of the completeness of the Milky Way sample (Koposov et al. 2008; Tollerud et al. 2008, and refs. therein) have reduced the deficit of *observed* satellites, to the point of qualitative agreement with the prediction of the model of Benson et al. (2002b). At issue now is the quality (rather than the lack) of agreement between such models and the data. We pay particular attention to the suppressive effect of photoheating. This is a significant process for shaping the faint end of the satellite luminosity function when, as we assume here, the strength of supernova feedback is fixed by constraints on the galaxy population as a whole.

2.2.1 Reionization and the satellite luminosity function

A simple model of reionization heating based on a halo mass dependent cooling threshold (Benson et al. 2003) is implemented in the Bower et al. (2006) model of GALFORM. This threshold is set by parameters termed V_{cut} and z_{cut}. No gas is allowed to cool within haloes having a circular velocity below V_{cut} at redshifts below z_{cut}. To good approximation, this scheme reproduces the link between the suppression of cooling and the evolution of the 'filtering mass' (as defined by Gnedin 2000) found in the more detailed model of Benson et al. (2002b), where photoheating of the intergalactic medium was modelled explicitly. In practice, in this simple model, the value of V_{cut} is most important. Variations in z_{cut} within plausible bounds have a less significant effect on the $z = 0$ luminosity function.

As stated above, we adopt as a fiducial model the GALFORM implementation and parameters of Bower et al. (2006). However, we make a single parameter change, lowering the value of V_{cut} from $50 \, \mathrm{km \, s^{-1}}$ to $30 \, \mathrm{km \, s^{-1}}$. This choice is motivated by recent *ab initio* cosmological galaxy formation simulations incorporating the effects of photoionization self-consistently (Hoeft et al. 2006; Okamoto, Gao & Theuns 2008; Okamoto & Frenk 2009; Okamoto et al. 2009). These studies find that values of $V_{cut} \sim 25 - 35 \, \mathrm{km \, s^{-1}}$ are preferable to the higher value suggested by the results of Gnedin (2000) and adopted in previous semi-analytic models (e.g. Somerville 2002; Bower et al. 2006; Croton et al. 2006; Li, De Lucia & Helmi 2009a). Altering this value affects only the very faint end of the galaxy luminosity function, and so does not change the results of (Bower et al. 2006). The choice of a fiducial set of semi-analytic parameters in this paper illustrates the flexibility of our approach to modelling stellar haloes. The N-body component of our models – Aquarius – represents a considerable investment of computational time. In contrast, the semi-analytic post-processing can be re-run in only a few hours, and can be easily 'upgraded' (by adding physical processes and constraints) in order to provide more detailed output, explore the consequences of parameter variations, or compare alternative semi-analytic models.
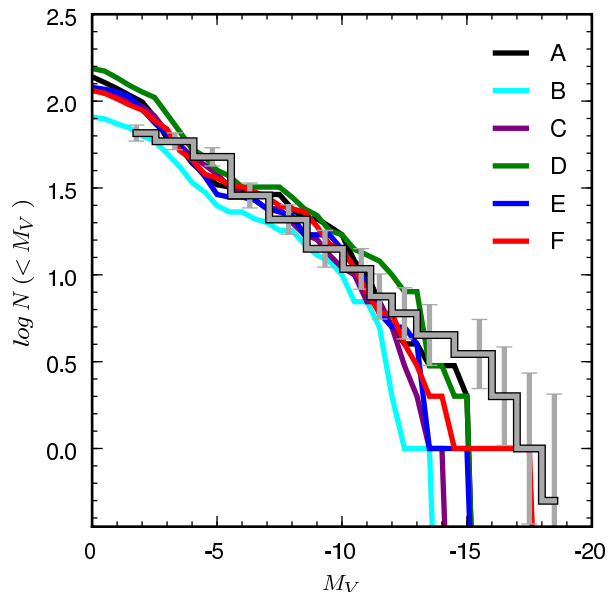

Figure 1. The cumulative *V*-band luminosity functions (LFs) of satellite galaxies for the six Aquarius haloes, adopting in GALFORM the parameters of Bower et al. (2006) with $V_{cut} = 30 \, \mathrm{km \, s^{-1}}$. These LFs *include* the effects of tidal stripping measured from our assignment of stars to dark matter particles (Section 3), although this makes only a small difference to the LF from our semi-analytic model alone. All galaxies within 280 kpc of the halo centre are counted as satellites (the total number of contributing satellites in each halo is indicated in the legend). The stepped line (grey, with error bars) shows the observed mean luminosity function found by Koposov et al. (2008) for the MW and M31 satellite system (also to 280 kpc), assuming an NFW distribution for satellites in correcting for SDSS sky coverage and detection efficiency below $M_v = -10$. The colour-coding of our haloes in this figure is used throughout.

The *V*-band satellite luminosity function resulting from the application of the GALFORM model described above to each Aquarius halo is shown in Fig. 1. Satellites are defined as all galaxies within a radius of 280 kpc from the centre of potential in the principal halo, equivalent to the limiting distance of the Koposov et al. (2008) completeness-corrected observational sample. These luminosity functions are measured from the *particle* realisations of satellites that we describe in the following section, and not directly from the semi-analytic model. They therefore account for the effects of tidal stripping, although these are minor: the fraction of satellites brighter than $M_V = -10$ is reduced very slightly in some of the haloes. In agreement with the findings of Benson et al. (2002a), the model matches the faint end of the luminosity function well, but fewer bright satellites are found in each of our six models than are observed in the mean of the Milky Way + M31 system, although the number of objects concerned is small. The true abundance of bright satellites for Milky Way-mass hosts is poorly constrained at present, so it is unclear whether or not this discrepancy reflects cosmic variance, a disparity in mass between the Aquarius haloes and the Milky Way halo, or a shortcoming of our fiducial Bower et al. (2006) model. A modification of this model in which the tidal stripping of hot gas coronae around infalling satellites is explicitly calculated (rather than assuming instantaneous removal; see Font et al. 2008) produces an acceptable abundance of bright satellites.

2.2.2 Further details

Within GALFORM, cold gas is transferred from tidally destroyed satellites to the disc of the central galaxy when their host subhaloes are no longer identified at the resolution limit imposed by SUB-FIND. In the Aq-2 simulations this corresponds to a minimum resolved dark halo mass of $\sim 3 \times 10^5 M_\odot$. In the GALFORM model of Bower et al. (2006), which does not include tidal stripping or a 'stellar halo' component, the satellite galaxy is considered to be fully disrupted (merged) at this point: its stars are transferred to the bulge component of the central galaxy. By contrast, our particle representation (described in Section 3) allows us to follow the *actual* fate of the satellite stars independently of this choice in the semi-analytic model. This choice is therefore largely a matter of 'book-keeping'; we have ensured that adopting this approach does not prematurely merge galaxies in the semi-analytic model that are still capable of seeding new stellar populations into the particle representation. Semi-analytic models based on N-body simulations often choose to 'follow' satellites with dark haloes falling below the numerical resolution by calculating an appropriate merger time-scale from the last-known N-body orbital parameters, accounting for dynamical friction. However, the resolution of Aquarius is sufficiently high to make a simpler and more self-consistent approach preferable in this case, preserving the one-to-one correspondence between star-forming semi-analytic galaxies and bound objects in the simulation. We have checked that allowing semi-analytic galaxies to survive without resolved subhaloes, subject to the treatment of dynamical friction used by Bower et al. (2006), affects only the faintest ($M_v \sim 0$) part of the survivor luminosity function. The true nature and survival of these extremely faint sub-resolution galaxies remains an interesting issue to be addressed by future semi-analytic models of galactic satellites.

In Table 2 (Section 4) we list the *V*-band magnitudes and total stellar masses of the central galaxies that form in the six Aquarius haloes. A wide range is evident, from an M31-analogue in halo Aq-C, to an M33-analogue in Aq-E. This is not unexpected: the Aquarius dark haloes were selected only on their mass and isolation, and these criteria alone do not guarantee that they will host close analogues of the Milky Way. The scaling and scatter in the predicted relationship between halo mass and central galaxy stellar mass are model-dependent. With the GALFORM parameter values of Bower et al., the mean central stellar mass in a typical Aquarius halo ($M_{\rm halo} \sim 1.4 \times 10^{12} M_\odot$) is $\sim 1.5 \times 10^{10} M_\odot$, approximately a factor of 3–4 below typical estimates of the stellar mass of the Milky Way ($\sim 6 \times 10^{10} M_\odot$ Flynn et al. 2006); the scatter in $M_{\rm gal}$ for our central galaxies reflects the overall distribution produced by the model of Bower et al. (2006) for haloes of this mass. The model of De Lucia et al. (2006), which like the Bower et al. (2006) model was constrained using statistical properties of bright field and cluster populations, produces a mean central stellar mass of $\sim 4 \times 10^{10} M_\odot$ for the typical halo mass of the Aquarius simulations, as well as a smaller scatter about the mean value.

In light of these modelling uncertainties and observational uncertainties in the determination of the true Milky Way dark halo mass to this precision, we choose not to scale the Aquarius haloes to a specific mass for 'direct' comparison with the Milky Way. The results we present concerning the assembly and structure of stellar haloes and the ensemble properties of satellite systems should not be sensitive to whether or not their galaxies are predicted to be direct analogues of the Milky Way by the Bower et al. (2006) GALFORM model. Therefore, in interpreting the *absolute* values of quantities compared to observational data in the following sections,

it should be borne in mind that we model a *range* of halo masses that could lie somewhat below the likely Milky Way value.

The Bower et al. (2006) implementation of GALFORM results in a mass-metallicity relation for faint galaxies which is slightly steeper than that derived from the satellites of the Milky Way and M31 (e.g. Mateo 1998; Kirby et al. 2008; see also Tremonti et al. 2004 and refs. therein). This results in model galaxies being on average ~ 0.5 dex more metal-poor in [Fe/H] than the observed relation at magnitudes fainter than $M_{\rm V} \sim -10$. Whilst it would be straightforward to make *ad hoc* adjustments to the model parameters in order to match this relation, doing so would violate the agreement established between the Bower et al. (2006) parameter set and a wide range of statistical constraints from the bright ($M_V < -19$) galaxy population.

3 BUILDING STELLAR HALOES

3.1 Assigning Stars To Dark Matter

Observations of the stellar velocity distributions of dwarf spheroidal satellites of the Milky Way imply that these objects are dispersion-supported systems with extremely high mass-to-light ratios, of order 10–1000 (e.g. Mateo 1998; Simon & Geha 2007; Strigari et al. 2007; Wolf et al. 2009; Walker et al. 2009). As we describe in this section, in order to construct basic models of these high-M/L systems without simulating their baryon dynamics explicitly, we will assume that their stars are formed 'dynamically coupled' to a strongly bound fraction of their dominant dark matter component, and will continue to trace that component throughout the simulation. Here we further assume that the depth at which stars form in a halo potential well depends only on the total mass of the halo. While these assumptions are too simplistic a description of stellar dynamics in such systems to compare with detailed structural and kinematic observations, we show that they none the less result in half-light radii and line-of-sight velocity dispersions in agreement with those of Milky Way dwarf spheroidals. Hence the disruption of a fraction of these model satellites by tidal forces in the main halo should reproduce stellar halo components ('streams') at a level of detail sufficient for an investigation of the assembly and gross structure of stellar haloes. We stress that these comparisons are used as constraints on the single additional free parameter in our model, and are not intended as predictions of a model for the satellite population.

In the context of our GALFORM model, the stellar content of a single galaxy can be thought of as a superposition of many distinct stellar populations, each defined by a particular formation time and metallicity. Although the halo merger tree used as input to GAL-FORM is discretized by the finite number of simulation outputs (snapshots), much finer interpolating timesteps are taken between snapshots when solving the differential equations governing star formation. Consequently, a large number of distinct populations are 'resolved' by GALFORM. However, we can update our particle (dynamical) data (and hence, can assign stars to dark matter) only at output times of the pre-existing N-body simulation. For the purposes of performing star-to-dark-matter assignments we reduce the fine-grained information computed by GALFORM between one output time and the next to a single aggregated population of 'new stars' formed at each snapshot.

As discussed above and in Section 1, we adopt the fundamental assumption that the motions of stars can be represented by dark matter particles. The aim of our method here is to select a sample

of representative particles from the parent N-body simulation to trace *each such stellar population*, individually. We describe first the general objective of our selection process, and then examine the selection criteria that we apply in practice.

Consider first the case of a single galaxy evolving in isolation. At a given simulation snapshot (B) the total mass of new stars formed since the previous snapshot (A) is given by the difference in the stellar mass of the semi-analytic galaxy recorded at each time,

$$\Delta M_\star^{AB} = M_\star^B - M_\star^A. \tag{1}$$

In our terminology, $\Delta M_\star^{AB}$ is a single stellar population (we do not track the small amount of mass lost during subsequent stellar evolution). The total mass in metals within the population is determined in the same way as the stellar mass; we do not follow individual chemical elements. In a similar manner, the luminosity of the new population (at $z = 0$) is given by the difference of the total luminosities (after evolution to $z = 0$) at successive snapshots.

From the list of particles in the simulation identified with the dark matter halo of the galaxy at B, we select a subset to be tracers of the stellar population $\Delta M_\star^{AB}$. Particles in this tracer set are 'tagged', i.e. are identified with data describing the stellar population. In the scheme we adopt here, equal 'weight' (fraction of stellar mass, luminosity and metals in $\Delta M_\star^{AB}$) is given to each particle in the set of tracers. We repeat this process for all snapshots, applying the energy criterion described below to *select a new set of DM tracers each time new stars are formed* in a particular galaxy. In this scheme, the same DM particle can be selected as a tracer at more than one output time (i.e. the same DM particle can be tagged with more than one stellar population). Hence a given DM particle accumulates its own individual star formation history. The dynamical evolution of satellite haloes determines whether or not a particular particle is eligible for the assignment of new stars during any given episode of star formation.

So far we have considered an 'isolated' galaxy. In practice, we apply this technique to a merger tree, in which a galaxy grows by the accretion of satellites as well as by *in situ* star formation. In the expression above, the total stellar mass at A, $M_\star^A$, is simply modified to include a sum over N immediate progenitor galaxies in addition to the galaxy itself i.e.,

$$\Delta M_\star^{AB} = M_\star^B - M_{\star,0}^A - \sum_{i>0} M_{\star,i}^A \tag{2}$$

where $M_{\star,0}^A$ represents the galaxy itself and $M_{\star,i}^A$ is the total stellar mass (at A) of the i'th progenitor deemed to have merged with the galaxy in the interval AB. Stars forming in the progenitors during the interval AB and stars forming in the galaxy itself are treated as a single population.

There is a one-to-one correspondence between a galaxy and a dark matter structure (halo or subhalo) from which particles are chosen as tracers of its newly formed stars. As discussed in Section 2.2, a satellite galaxy whose host subhalo is no longer identified by SUBFIND has its cold gas content transferred immediately to the central galaxy of their common parent halo and forms no new stars. In the semi-analytic model, the stars of the satellite are also added to the bulge component of the central galaxy. This choice is irrelevant in our particle representation, as we can track the actual fate of these stars.

3.2 Assignment criteria

3.2.1 Selection of dark matter particles

In this section we describe how we choose the dark matter particles within haloes that are to be tagged with a newly formed stellar population. In Section 1 we briefly described the particle-tagging method employed by Bullock & Johnston (2005), the philosophy of which we term '*in vitro*', using idealised initial conditions to simulate accretion events individually in a 'controlled' environment. By contrast, our approach is to *postprocess* fully cosmological simulations '*in vivo*'[2]. In a fully cosmological N-body simulation the growth of the central potential, the structure of the halo and the orbits, accretion times and tidal disruption of subhaloes are fully consistent with one another. The central potential is non-spherical (although no disc component is included in our dynamical model) and can grow violently as well as through smooth accretion. Our model is therefore applicable at high redshift when the halo is undergoing rapid assembly. The complexities in the halo potential realised in a fully cosmological simulation are likely to be an important influence on the dynamics of satellites (e.g. Sales et al. 2007a) and on the evolution of streams, through phase-mixing and orbital precession (e.g. Helmi & White 1999).

We approach the selection of dark matter particles for stellar tagging differently to Bullock & Johnston (2005), because we are postprocessing a cosmological N-body simulation rather than constructing idealised initial conditions for each satellite. Rather than assigning the mass-to-light ratio of each tagged particle by comparing stellar and dark matter energy distribution functions in the halo concerned, we assume that the energy distribution of newly formed stars traces that of the dark matter. We order the particles in the halo by binding energy[3] and select a most-bound fraction f_{MB} to be tagged with newly-formed stars. As previously described, stars are shared equally among the selected DM particles.

Our approach implies a rather simple dynamical model for stars in satellite galaxies. However, the main results of this paper do not concern the satellites themselves; instead we focus on the debris of objects that are totally (or largely) disrupted to build the stellar halo. As we describe below, we compare the structure and kinematics of our model satellites (those that survive at $z = 0$) to Local Group dwarf galaxies in order to fix the value of the free parameter, f_{MB}. Since we impose this constraint, our method cannot predict these satellite properties *ab initio*. Constraining our model in this way ensures reasonable structural properties in the population of progenitor satellites, and retains full predictive power with regard to the stellar halo. More complex models would, of course, be possible, in which f_{MB} is not a free parameter but is instead physically determined by the semi-analytic model. It would also be possible to use a more complicated tagging scheme to attempt to represent, for example, star formation in a disc. However, such models would add substantial complexity to the method and there are currently very few observational constraints on how stars were formed in satellite galaxies. Thus, we believe that a simple model suffices for our present study of the stellar halo.

Our approach has similarities with that of De Lucia & Helmi

---

[2] This terminology should not be taken to imply that 'star particles' themselves are included in the N-body simulation; here stellar populations are simply tags affixed to dark matter particles.

[3] Here, the most bound particle is that with the most negative total energy, including both kinetic and gravitational contributions. Binding energies are computed relative to the bound set of particles comprising an object identified by SUBFIND.
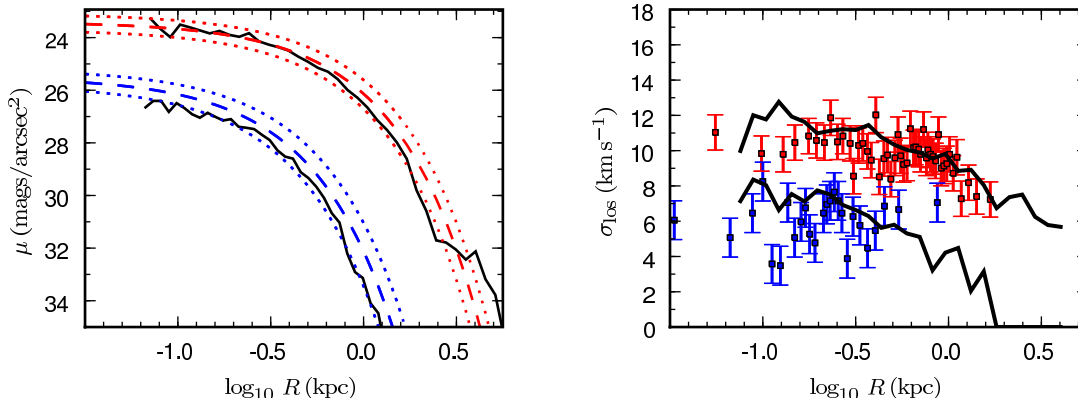
Figure 2. Examples of individual satellites in our models (solid black lines), compared to Fornax (red) and Carina (blue), showing surface brightness (left, Irwin & Hatzidimitriou 1995) and line-of-sight velocity dispersion (right, Walker et al. 2009). With our fiducial GALFORM model, simultaneous matches to both $\sigma(R)$ and $\mu(R)$ for these datasets are found only among satellites that have undergone substantial tidal stripping (see text).

(2008), who tag the most bound 10% of particles in satellite haloes with stars. However, De Lucia & Helmi perform this tagging only *once* for each satellite, at the time at which its parent halo becomes a subhalo of the main halo (which we refer to as the time of infall[4]). Both this approach and that of Bullock & Johnston (2005) define the end result of the previous dynamical evolution of an infalling satellite, the former by assuming light traces dark matter and the latter with a parameterized King profile.

As described above, in our model each newly-formed stellar population is assigned to a subset of DM particles, chosen according to the 'instantaneous' dynamical state of its host halo. This choice is independent of any previous star formation in the same halo. It is the dynamical evolution of these many tracer sets in each satellite that determines its stellar distribution at any point in the simulation.

Implementing a particle-tagging scheme such as this within a fully cosmological simulation requires a number of additional issues to be addressed, which we summarise here.

(i) *Subhalo assignments*: Star formation in a satellite galaxy will continue to tag particles regardless of the level of its halo in the hierarchy of bound structures (halo, subhalo, subsubhalo etc.). The growth of a dark matter halo ends when it becomes a subhalo of a more massive object, whereupon its mass is reduced through tidal stripping. The assignment of stars to particles in the central regions according to binding energy should, of course, be insensitive to the stripping of dark matter at larger radii. However, choosing a fixed fraction of dark matter tracer particles to represent new stellar populations couples the mass of the subhalo to the number of particles chosen. Therefore, when assigning stars to particles in a subhalo, we instead select a fixed *number* of particles, equal to the number constituting the most-bound fraction f_{MB} of the halo at the time of infall.

(ii) *Equilibrium criterion*: To guard against assigning stars to sets of tracer particles that are temporarily far from dynamical equilibrium, we adopt the conservative measure of deferring assignments to any halo in which the centres of mass and potential are separated by more than 7% of the half-mass radius $r_{1/2}$. We

select $0.07\,r_{1/2}$ in accordance with the criterion of $0.14\,r_{vir}$ used to select relaxed objects in the study of Neto et al. (2007), taking $r_{vir} \sim 2\,r_{1/2}$. These deferred assignments are carried out at the next snapshot at which this criterion is satisfied, or at the time of infall into a more massive halo.

(iii) *No in situ star formation*: Stars formed in the main galaxy in each Aquarius simulation (identified as the central galaxy of the most massive dark halo at $z = 0$) are never assigned to DM particles. This exclusion is applied over the entire history of that galaxy. Stars formed in situ are likely to contribute to the innermost regions of the stellar halo, within which they may be redistributed in mergers. However, the dynamics of stars formed in a dissipationally-collapsed, baryon-dominated thin disc cannot be represented with particles chosen from a dark matter-only simulation. We choose instead to study the accreted component in isolation. Our technique none the less offers the possibility of extracting *some* information on a fraction of in situ stars were we to assign them to dark matter particles (those contributing to the bulge or forming at early times, for example). We choose to omit this additional complexity here. SPH simulations of stellar haloes (which naturally model the in situ component more accurately than the accreted component) suggest that the contribution of in situ stars to the halo is small beyond ~ 20 kpc (Abadi et al. 2006; Zolotov et al. 2009).

At early times, when the principal halo in each simulation is growing rapidly and near-equal-mass mergers are common, the definition of the 'main' branch of its merger tree can become ambiguous. Also, the main branch of the galaxy merger tree need not follow the main branch of the halo tree. Hence, our choice of which branch to exclude (on the basis that it is forming 'in situ' stars) also becomes ambiguous; indeed, it is not clear that any of these 'equivalent' early branches should be excluded. Later we will show that two of our haloes have concentrated density profiles. We have confirmed that these *do not* arise from making the 'wrong' choice in these uncertain cases, i.e. from tagging particles in the dynamically robust core of the 'true' main halo. Making a different choice of the excluded branch in these cases (before the principal branch can be unambiguously identified) simply replaces one of these concentrated components with another very similar component. Therefore, we adopt the above definition of the galaxy main branch when excluding in situ stars.

---

[4] In both Bullock & Johnston (2005) and De Lucia & Helmi (2008) only satellites directly accreted by the main halo 'trigger' assignments to dark matter; the hierarchy of mergers/accretions forming a directly-infalling satellite are subsumed in that single assignment.

3.2.2 Individual satellites

We show in the following section that with a suitable choice of the most-bound fraction, our method produces a population of model satellites at $z = 0$ having properties consistent with observed relationships between magnitude, half-light radius/surface brightness and velocity dispersion for satellite populations of the Milky Way and M31. In Fig. 2 we show profiles of surface brightness and velocity dispersion for two individual satellites from these models at $z = 0$, chosen to give a rough match to observations of Fornax and Carina. This suggests that our galaxy formation model and the simple prescription for the spatial distribution of star formation can produce realistic stellar structures within dark haloes. However, while it is possible to match these individual observed satellites with examples drawn from our models, we caution that we can only match their observed surface brightness and velocity dispersion profiles *simultaneously* by choosing model satellites that have suffered substantial tidal stripping. This is most notable in the case of our match to Fornax, which retains only 2% of its dark matter relative to the time of its accretion to the main halo, and 20% of its stellar mass. However, as we show in Section 4.2, the majority of massive surviving satellites have not suffered substantial tidal stripping.

We have tested our method with assignments for each satellite delayed until the time of infall, as in De Lucia & Helmi (2008). This results in slightly more compact galaxies than in our standard *in vivo* approach, where mergers and tidal forces (and relaxation through two-body encounters for objects near the resolution limit) can increase the energies of tagged dark matter particles. However, we find that this makes little difference to the results that we discuss below.

3.2.3 Parameter constraints and convergence

We now compare the $z = 0$ satellite populations of our models with trends observed in the dwarf companions of the Milky Way and M31 in order to determine a suitable choice of the fixed fraction, f_{MB}, of the most bound dark matter particles selected in a given halo. Our aim is to study the stellar halo, and therefore we use the sizes of our surviving satellites as a constraint on f_{MB} and as a test of convergence. Within the range of f_{MB} that produces plausible satellites, the gross properties of our haloes, such as total luminosity, change by only a few percent.

In Fig. 3, we show the relationship between the absolute magnitudes, M_V, of satellites (combining data from two of our simulations, Aq-A and Aq-F), and the projected radius enclosing one half of their total luminosity, which we refer to as the effective radius, r_{eff}. We compare our models to a compilation of dwarf galaxy data in the Local Group, including the satellites of the Milky Way and M31. The slope of the median relation for our satellites agrees well with that of the data for the choices $f_{MB} = 1\%$ and 3%. It is clear that a choice of 5% produces bright satellites that are too extended, while for 0.5% they are too compact. We therefore prefer $f_{MB} = 1\%$. A more detailed comparison to the data at this level is problematic: the observed sample of dwarf galaxies available at any given magnitude is small, and the data themselves contain puzzling features such as an apparently systematic difference in size between the bright Milky Way and M31 satellites.

Fig. 3 also shows (as dotted lines) the same results for our model run on the lower-resolution simulations of haloes Aq-A and Aq-F. The particle mass in the Aq-3 series is approximately three times greater than in Aq-2, and the force softening scale is larger
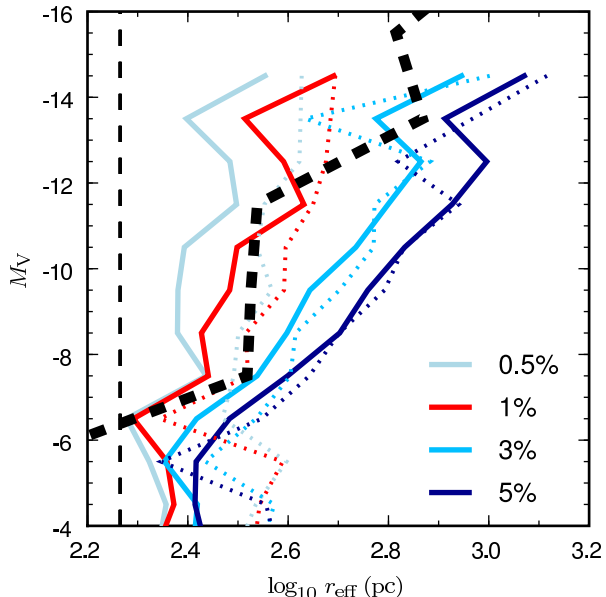

Figure 3. Median effective radius r_{eff} (enclosing half of the total luminosity in projection) as a function of magnitude for model satellites in haloes Aq-A and Aq-F at $z = 0$. A thin vertical dashed line indicates the softening scale of the simulation: r_{eff} is unreliable close to this value and meaningless below it. *Thick lines* represent our higher-resolution simulations (Aq-2) using a range of values of the fraction of most bound particles chosen in a stellar population assignment, f_{MB}. *Dotted lines* correspond to lower resolution simulations (Aq-3) of the same haloes. A *thick dashed line* shows the corresponding median of observations of Local Group dwarf galaxies. These galaxies, and our model data points for all haloes in the Aq-2 series with $f_{MB} = 1\%$, are plotted individually in Fig. 4.

by a factor of two. We concentrate on the convergence behaviour of our simulations for galaxies larger than the softening length, and also where our sample provides a statistically meaningful number of galaxies at a given magnitude; this selection corresponds closely to the regime of the brighter dwarf spheroidal satellites of the Milky Way and M31, $-15 < M_V < -5$. In this regime, Fig. 3 shows convergence of the median relations brighter than $M_V = -5$ for $f_{MB} = 3\%$ and 5%. The case for $f_{MB} = 1\%$ is less clear-cut. The number of particles available for a given assignment is set by the mass of the halo; haloes near the resolution limit (with ~ 100 particles) will, of course, have only ~ 1 particle selected in a single assignment. In addition to this poor resolution, galaxies formed by such small-number assignments are more sensitive to spurious two-body heating in the innermost regions of subhaloes. We therefore expect the resulting galaxies to be dominated by few-particle 'noise' and to show poor convergence behaviour.

We adopt $f_{MB} = 1\%$ as a reasonable match to the data (noting also that it lies close to the power-law fit employed by Bullock & Johnston (2005) to map luminosities to satellite sizes). We believe the resulting satellites to be sufficiently converged at the resolution of our Aq-2 simulations with this choice of f_{MB} to permit a statistical study of the disrupted population represented by the stellar halo. In support of this assertion, we offer the following heuristic argument. The change in resolution from Aq-3 to Aq-2 results in approximately three times more particles being selected at fixed f_{MB}; likewise, a change in f_{MB} from 1% to 3% selects three times more particles at fixed resolution. Therefore, as $f_{MB} = 3\%$ has converged at the resolution of Aq-3, it is reasonable to expect that
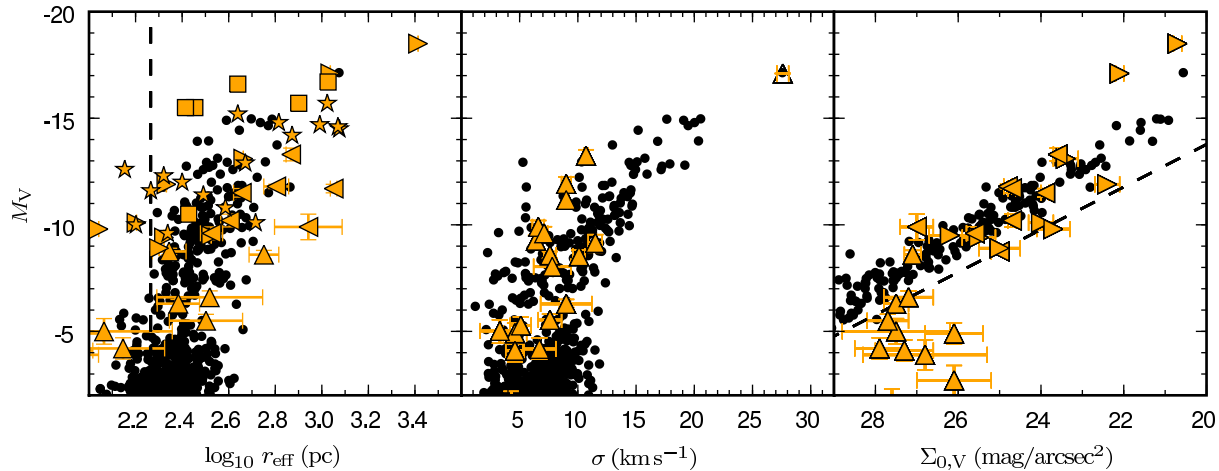
Figure 4. Projected half-light radius (left), mean luminosity-weighted 1D velocity dispersion (centre) and central surface brightness (right) of simulated satellite galaxies (defined by $r_{GC} < 280\,\mathrm{kpc}$) that survive in all haloes at $z = 0$, as a function of absolute V-band magnitude. Observational data for Milky Way and M31 satellites are shown as orange symbols; values are from Mateo (1998) and other authors as follows: bright satellites (triangles pointing right, Grebel, Gallagher & Harbeck 2003); faint MW satellites discovered since 2005 (triangles pointing up, Martin, de Jong & Rix 2008); M31 dwarf spheroidals (triangles pointing left, McConnachie et al. 2006; Martin et al. 2009); M31 ellipticals (squares); Local Group 'field' dwarf spheroidals and dwarf irregulars (stars). In the central panel we use data for Milky Way satellites only tabulated by Wolf et al. (2009) and for the SMC, Grebel et al. (2003). In the rightmost panel, we plot data for the Milky Way and M31 (Grebel et al. 2003; Martin et al. 2008). A dashed line indicates the surface brightness of an object of a given magnitude with $r_{eff} = 2.8\epsilon$, the gravitational softening scale (see Section 2.1).

$f_{MB} = 1\%$ selects a sufficient number of particles to ensure that satellite sizes are not dominated by noise at the resolution of Aq-2. We show below that the most significant contribution to the halo comes from a handful of well resolved objects with $M_V < -10$, rather than from the aggregation of many fainter satellites. Additionally, as demonstrated for example by Peñarrubia, McConnachie & Navarro (2008a); Peñarrubia, Navarro, & McConnachie (2008b); Peñarrubia et al. (2009), there is a 'knife-edge' between the onset of stellar stripping and total disruption for stars deeply embedded within the innermost few percent of the dark matter in a halo. We conclude that premature stripping resulting from an over-extension of very small satellites in our model is unlikely to alter the gross properties of our stellar haloes.

The points raised above in connection with Fig. 3 make clear that the *in vivo* particle tagging approach demands extremely high resolution, near the limits of current cosmological N-body simulations. The choice of $f_{MB} = 1\%$ in this approach (from an acceptable range of $1 - 3\%$) is not arbitrary. For example, a choice of $f_{MB} = 10\%$ (either as a round-number estimate,

For the remainder of this paper we concentrate on the higher resolution Aq-2 simulations. In Fig. 4 we fix f_{MB} at 1% and compare the surviving satellites from all six of our haloes with observational data for three properties correlated with absolute magnitude: effective radius, r_{eff}, mean luminosity-weighted line-of-sight velocity dispersion, σ, and central surface brightness, μ_0 (although the latter is not independent of r_{eff}). In all cases our model satellites agree well with the trends and scatter in the data brighter than $M_V = -5$.

The force softening scale of the simulation (indicated in the first and third panels by dashed lines) effectively imposes a maximum density on satellite dark haloes. At this radial scale we would expect r_{eff} to become independent of magnitude for numerical reasons: Fig. 4 shows that the $r_{eff}(M_V)$ relation becomes steeper for galaxies fainter than $M_V \sim -9$, corresponding to $r_{eff} \sim 200\,\mathrm{pc}$.

This resolution-dependent maximum density corresponds to a minimum surface brightness at a given magnitude. The low-surface-brightness limit in the Milky Way data shown in the right-hand panel of Fig. 4 corresponds to the completeness limit of current surveys (e.g. Koposov et al. 2008; Tollerud et al. 2008). The lower surface brightness satellite population predicted by our model is not, in principle, incompatible with current data.

In Fig. 5 we show the relationship between total luminosity and the mass of dark matter enclosed within 300 pc, M_{300}, for our simulated satellites in all haloes. This radial scale is well-resolved in the level 2 Aquarius simulations (see also Font et al. 2009, in prep.). Our galaxies show a steeper trend than the data of Strigari et al. (2008), with the strongest discrepency (0.5 dex in M_{300}) for the brightest satellites. Nevertheless, both show very little variation, having $M_{300} \sim 10^7\,\mathrm{M_\odot}$ over five orders of magnitude in luminosity. In agreement with previous studies using semi-analytic models and lower-resolution N-body simulations (Macciò, Kang & Moore 2009; Busha et al. 2009; Li et al. 2009b; Koposov et al. 2009), and N-body gasdynamic simulations (Okamoto & Frenk 2009), we find that this characteristic scale arises naturally as a result of astrophysical processes including gas cooling, star formation and feedback.

3.3 Defining the stellar halo and satellite galaxies

To conclude this section, we summarise the terminology we adopt when describing our results. Tagged dark matter particles in the self-bound haloes and subhaloes identified by SUBFIND constitute our 'galaxies'. Our stellar haloes comprise all tagged particles bound to the main halo in the simulation, along with those tagged particles not in any bound group (below we impose an additional radial criterion on our definition of the stellar halo). All galaxies within 280 kpc of the centre of the main halo are classed as 'satellites', as in the luminosity functions shown in Fig. 1. Centres of mass of the stellar haloes and satellites are determined from
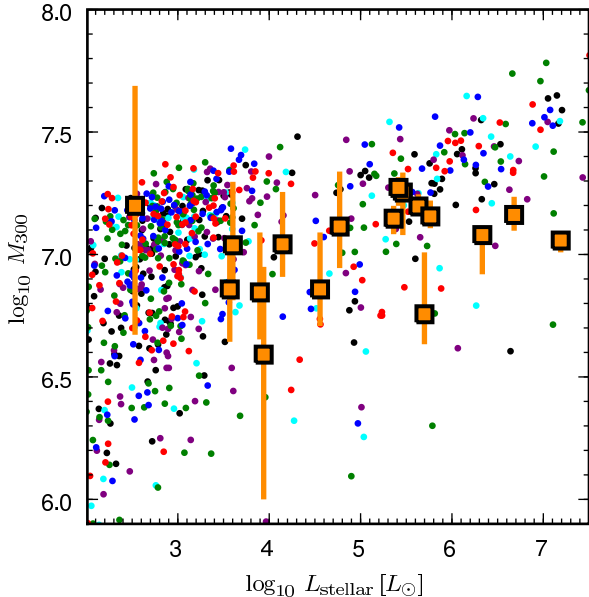
Figure 5. Mass in dark matter enclosed within 300 pc (M_{300}) as a function of luminosity (V-band) for satellites in each of our simulated haloes (coloured points, colours as Fig. 1). Maximum likelihood values of M_{300} for Milky Way dwarf spheroidals from Strigari et al. (2008) are shown (orange squares), with error bars indicating the range with likelihood greater than 60.6% of the maximum.

tagged particles only, using the iterative centring process described by Power et al. (2003).

Many structural elements of a galaxy intermix within a few kiloparsecs of its centre, and attempts to describe the innermost regions of a stellar halo require a careful and unambiguous definition of other components present. This is especially important when distinguishing between those components that are represented in our model and those that are not. Therefore, before describing our haloes[5], we first summarise some of these possible sources of confusion, clarify what is and is not included in our model, and define a range of galactocentric distances on which we will focus our analysis of the stellar halo.

As discussed above, our model does not track with particles any stars formed in situ in the central 'Milky Way' galaxy, whether in a rotationally supported thin disc or otherwise (this central galaxy is, of course, included in the underlying semi-analytic model). We therefore refer to the halo stars that *are* included in our model as *accreted* and those that form in the central galaxy (and hence are *not* explicitly tracked in our model) as *in situ*. Observational definitions of the 'stellar halo' typically do not attempt to distinguish between accreted and in situ stars, only between components separated empirically by their kinematic, spatial and chemical properties.

The 'contamination' of a purely-accreted halo by stars formed in situ is likely to be most acute near the plane of the disc. Observations of the Milky Way and analogous galaxies frequently distinguish a 'thick disc' component (Gilmore & Reid 1983; Carollo et al. 2009) thought to result either from dynamical heating of the thin disc by minor mergers (e.g. Toth & Ostriker 1992; Quinn,

Hernquist & Fullagar 1993; Velazquez & White 1999; Font et al. 2001; Benson et al. 2004; Kazantzidis et al. 2008) or from accretion debris (Abadi et al. 2003; Yoachim & Dalcanton 2005, 2008). The presence of such a component in M31 is unclear: an 'extended disc' is observed (Ibata et al. 2005), which rotates rapidly, contains a young stellar population and is aligned with the axes of the thin disc, but extends to ~ 40 kpc and shows many irregular morphological features suggestive of a violent origin. In principle, our model will follow the formation of accreted thick discs. However, the stars in our model only feel the potential of the dark halo; the presence of a massive baryonic disc could significantly alter this potential in the central region and influence the formation of an accreted thick disc (e.g. Velazquez & White 1999).

Our models include that part of the galactic bulge built from accreted stars, but none of the many other possible processes of bulge formation (starbursts, bars etc.). However, the interpretation of this component, the signatures of an observational counterpart and the extent to which our simulation accurately represents its dynamics are all beyond the scope of this paper. Instead, we will consider stars within 3 kpc of the dark halo potential centre as 'accreted bulge', and define those between 3 kpc and a maximum radius of 280 kpc as the 'stellar halo' on which we will focus our analysis. This arbitrary radial cut is chosen to exclude the region in which the observational separation of 'bulge' and 'halo' stars is not straightforward, and which is implicitly excluded from conventional observational definitions of the halo. It is *not* intended to reflect a physical scale-length or dichotomy in our stellar haloes, analogous to that claimed for the Milky Way (e.g. Carollo et al. 2007, 2009). Beyond 3 kpc we believe that the ambiguities discussed above and the 'incompleteness' of our models with regard to stars formed *in situ* should not substantially affect the comparison of our *accreted* stars with observational data.

4   RESULTS: THE AQUARIUS STELLAR HALOES

In this section, we present the six stellar haloes resulting from the application of the method described above to the Aquarius simulations. Here our aim is to characterise the assembly history of the six haloes and their global properties. Quantities measured for each halo are collected in Table 2. These include a measure of the number of progenitor galaxies contributing to the stellar halo, N_{prog}. This last quantity is not the total number of accreted satellites, but instead is defined as $N_{\mathrm{prog}} = M_{\mathrm{halo}}^2 / \sum_i m_{\mathrm{prog,i}}^2$ where $m_{\mathrm{prog,i}}$ is the stellar mass contributed by the i'th progenitor. N_{prog} is equal to the total number of progenitors in the case where each contributes equal mass, or to the number of significant progenitors in the case where the remainder provide a negligible contribution.

4.1   Visualisation in projection

A 300×300 kpc projected surface brightness map of each stellar halo at $z = 0$ is shown in Fig. 6. Substantial diversity among the six haloes is apparent. Haloes Aq-B and Aq-E are distinguished by their strong central concentration, with few features of detectable surface brightness beyond ~ 20 kpc. Haloes Aq-A, Aq-C, Aq-D and Aq-F all show more extended envelopes to 75-100 kpc; each envelope is a superposition of streams and shells that have been phase-mixed to varying degrees.

Analogues of many morphological features observed in the halo of M31 (Ibata et al. 2007; Tanaka et al. 2009; McConnachie et al. 2009) and other galaxies (e.g. Martínez-Delgado et al. 2008)
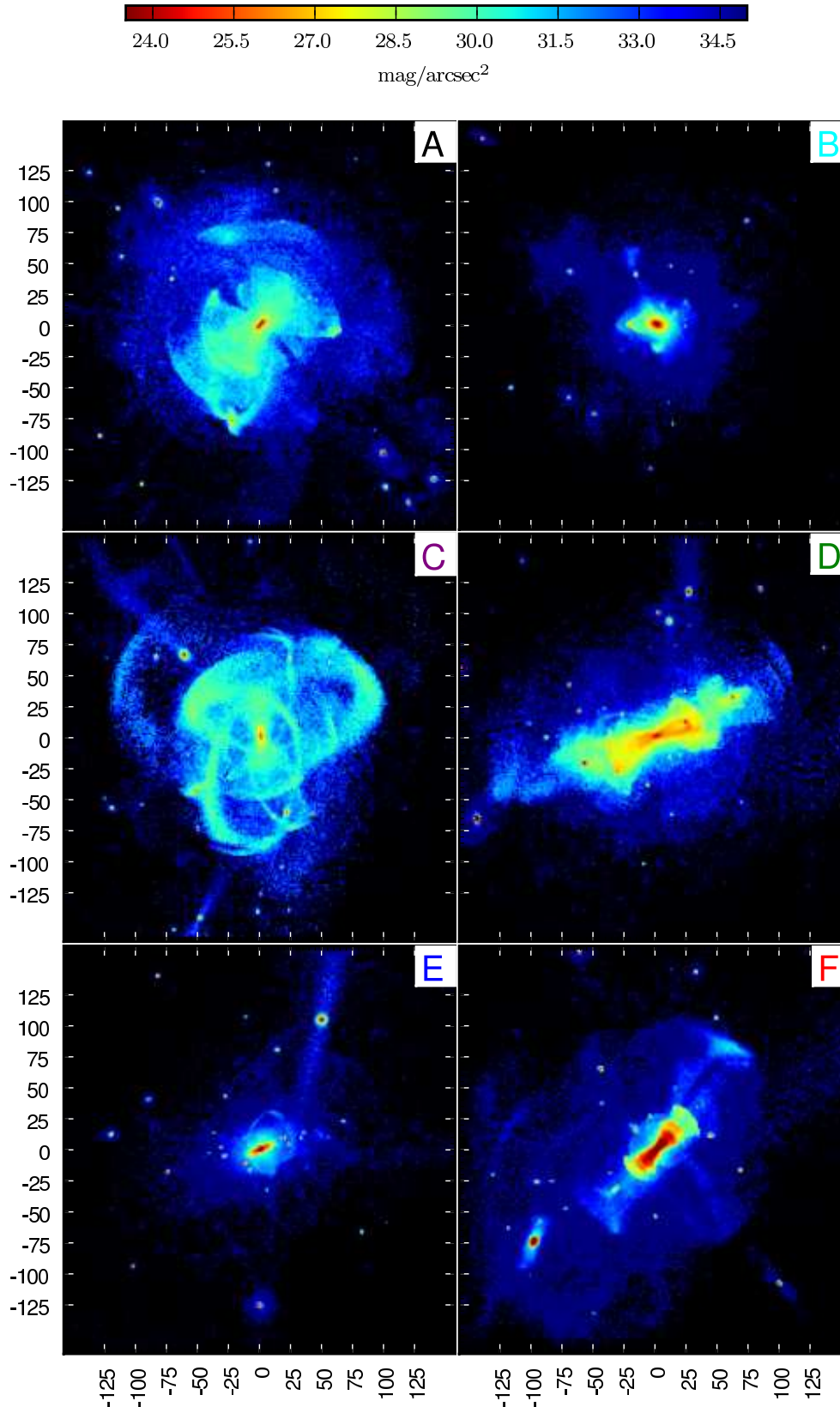
---

[5] We explicitly distinguish between the stellar halo and the dark halo in ambiguous cases; typically the former is implied throughout

Figure 6. *V*-band surface brightness of our model haloes (and surviving satellites), to a limiting depth of $35\,\mathrm{mag/arcsec}^2$. The axis scales are in kiloparsecs. Only stars formed in satellites are present in our particle model; there is no contribution to these maps from a central galactic disc or bulge formed in situ (see Section 3.3)
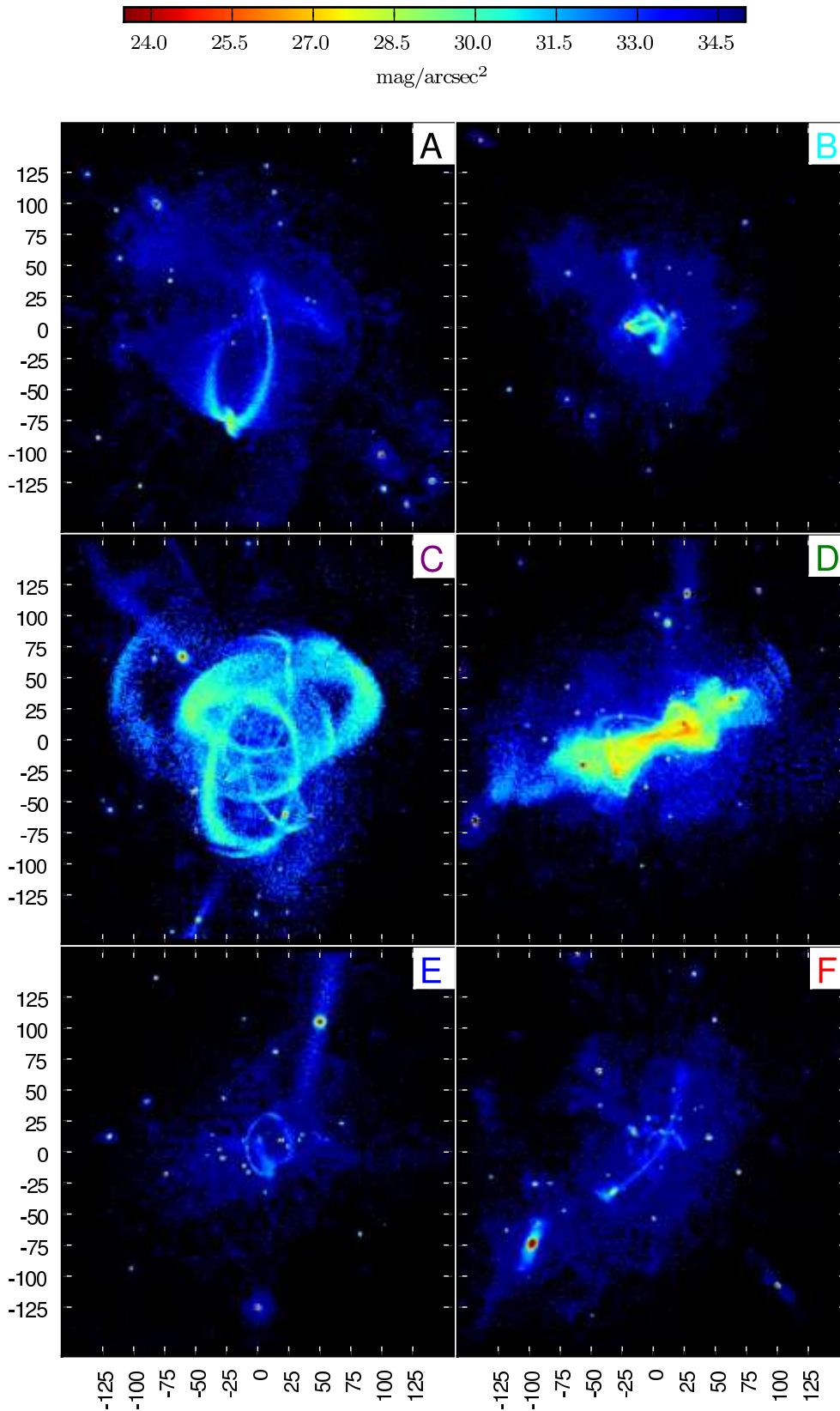
Figure 7. As Fig. 6, but here showing only those stars stripped from satellites that survive at $z = 0$

Table 2. For each of our simulated haloes we tabulate: the luminosity and mass of halo stars (in the range $3 < r < 280$ kpc); the mass of accreted bulge stars ($r < 3$ kpc); the total stellar mass and V-band magnitude of the central galaxy in GALFORM; the number of surviving satellites (brighter than $M_V = 0$); the fraction of the total stellar mass within 280 kpc bound in surviving satellites at $z = 0$, $f_{\rm sat}$; the fraction of *halo* stellar mass ($r < 280$ kpc) contributed by these surviving satellites, $f_{\rm surv}$; the number of halo progenitors, $N_{\rm prog}$ (see text); the half-light radius of the stellar halo ($r < 280$ kpc); the inner and outer slope and break radius of a broken power-law fit to the three-dimensional density profile of halo stars ($3 < r < 280$ kpc).

Halo	$L_{V,\rm halo}$ [$10^8 \rm L_\odot$]	$M_{\star,\rm halo}$ [$10^8 \rm M_\odot$]	$M_{\star,\rm bulge}$ [$10^8 \rm M_\odot$]	$M_{\rm gal}$ [$10^{10} \rm M_\odot$]	M_V	$N_{\rm sat}$	$f_{\rm sat}$	$f_{\rm surv}$	$N_{\rm prog}$	$r_{1/2}$ [kpc]	$n_{\rm in}$	$n_{\rm out}$	$r_{\rm brk}$ [kpc]
A	1.51	2.80	1.00	1.88	-20.3	161	0.61	0.065	3.8	20	-2.7	-8.2	80.4
B	1.27	2.27	3.33	1.49	-20.1	91	0.07	0.036	2.4	2.3	-4.2	-5.8	34.6
C	1.95	3.58	0.34	7.84	-21.3	150	0.28	0.667	2.8	53	-2.0	-9.4	90.8
D	5.55	9.81	1.32	0.72	-19.1	178	0.35	0.620	4.3	26	-2.0	-5.9	37.7
E	0.90	1.76	16.80	0.45	-18.6	135	0.11	0.003	1.2	1.0	-4.7	-4.4	15.2
F	17.34	24.90	6.42	1.36	-20.1	134	0.28	0.002	1.1	6.3	-2.9	-5.9	14.0

can be found in our simulations. For example, the lower left quadrant of Aq-A shows arc-like features reminiscent of a complex of 'parallel' streams in the M31 halo labelled A, B, C and D by Ibata et al. (2007) and Chapman et al. (2008), which have surface brightnesses of $30 - 33\,\rm mag\,arcsec^{-2}$ and a range of metallicities (Tanaka et al. 2009). These streams in Aq-A can also be traced faintly in the upper right quadrant of the image and superficially resemble the edges of 'shells'. In fact, they result from two separate progenitor streams, each tracing multiple wraps of decaying orbits (and hence contributing more than one 'arc' each). Seen in three dimensions, these two debris complexes (which are among the most significant contributors to the Aq-A halo) are elaborate and irregular structures, the true nature of which is not readily apparent in any given projection[6].

The brightest and most coherent structures visible in Fig. 6 are attributable to the most recent accretion events. To illustrate the contribution of recently-infalling objects (quantified in Section 4.2), we show the same projections of the haloes in Fig. 7, but include only those stars whose parent satellite survives at $z = 0$. In haloes Aq-C and Aq-D, stars stripped from surviving satellites constitute $\sim 60-70\%$ of the halo, while in the other haloes their contribution is $\lesssim 10\%$. Not all the recently-infalling satellites responsible for bright halo features survive; for example, the massive satellite that merges at $z \sim 0.3$ and produces the prominent set of 'shells' in Aq-F.

Fig. 6 shows that all our haloes are notably flattened, particularly in the central regions where most of their light is concentrated. Axial ratios $q = c/a$ and $s = b/a$ of three-dimensional ellipsoidal fits to halo stars within 10 kpc of the halo centre are given in Table 3 (these fits include stars within the accreted bulge region defined above). Most of our haloes are strongly prolate within 10 kpc. Halo Aq-E is very different, having a highly oblate (i.e. disc-like) shape in this region – this structure of ~ 20 kpc extent can be seen 'edge on' in Fig. 6 and can be described as an 'accreted thick disc' (e.g. Abadi et al. 2003; Peñarrubia, McConnachie & Babul 2006; Read et al. 2008). We defer further analysis of this interesting object to a subsequent paper. Beyond 10–30 kpc, the stellar mass in our haloes is not smoothly distributed but instead consists of a number of discrete streams, plumes and other irregular structures. Fits to all halo stars assuming a smoothly varying ellipsoidal distribution of mass

Table 3. Axial ratios $q = c/a$ and $s = b/a$ of stellar-mass-weighted three-dimensional ellipsoidal fits to halo stars within a galactocentric radius of 10 kpc. These were determined using the iterative procedure described by Allgood et al. (2006), which attempts to fit the shapes of self-consistent 'isodensity' contours. A spherical contour of $r = 10$ kpc is assumed initially; the shape and orientation of this contour are then updated on each iteration to those obtained by diagonalzing the inertia tensor of the mass enclosed (maintaining the length of the longest axis). The values thus obtained are slightly more prolate than those obtained from a single diagnonalization using all mass with a spherical contour (i.e. the first iteration of our approach), reflecting the extremely flattened shapes of our haloes at this radius. The oblate shape of Aq-E is not sensitive to this choice of method.

Halo	A	B	C	D	E	F
q_{10}	0.27	0.28	0.29	0.33	0.36	0.21
s_{10}	0.30	0.32	0.32	0.42	0.96	0.25

interior to a given radius do not accurately describe these sparse outer regions.

Few observations of stellar halo shapes are available for comparison with our models. M31 is the only galaxy in which a projected stellar halo has been imaged to a depth sufficient to account for a significant fraction of halo stars. Pritchet & van den Bergh (1994) measured a projected axial ratio for the M31 halo at ~ 10 kpc of ~ 0.5. Ibata et al. (2005) describe a highly irregular and rotating inner halo component or 'extended disc' (to $\sim 40\,\rm kpc$) of $27 - 31\,\rm mag/arcsec^2$, aligned with the thin disc and having an axial ratio ~ 0.6 in projection. Zibetti & Ferguson (2004) find a similar axial ratio for the halo of a galaxy at $z = 0.32$ observed in the Hubble ultra-deep field. Evidence for the universality of flattened stellar haloes is given by Zibetti, White & Brinkmann (2004), who find a best-fitting projected axial ratio of $\sim 0.5 - 0.7$ for the low surface brightness envelope of ~ 1000 stacked edge-on late-type galaxies in SDSS. A mildly *oblate* halo with $c/a \sim 0.6$ is reported for the Milky Way, with an increase in flattening at smaller radii (< 20 kpc; e.g. Chiba & Beers 2000; Bell et al. 2008; Carollo et al. 2007). Interestingly, Morrison et al. (2009) present evidence for a highly flattened halo ($c/a \sim 0.2$) component in the Solar neighbourhood, which appears to be dispersion-supported (i.e. kinematically *distinct* from a rotationally supported thick disc).

The shapes of components in our haloes selected by their kinematics, chemistry or photometry may be very different to those obtained from the aggregated stellar mass. A full comparison, accounting for the variety of observational selections, projection ef-

---

[6] Three orthogonal projections for each halo can be found at http://www.virgo.dur.ac.uk/aquarius
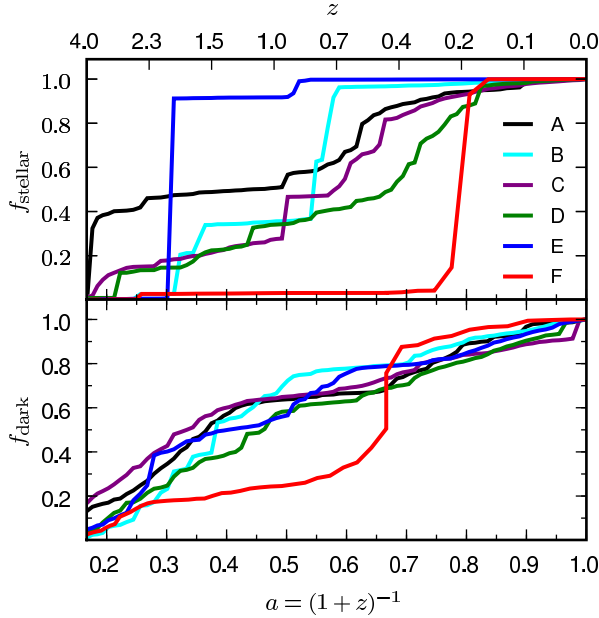
Figure 8. The growth of the stellar halo (*upper panel*) and the dark matter halo (the principal branch; *lower panel*) as a function of expansion factor (*bottom axis*) or redshift (*top axis*). Lines show the mass fraction of each halo in place at a given time. Stars are counted as belonging to the stellar halo when the DM particle that they tag is assigned to the principal halo, or is not bound to any SUBFIND group.

fects and definitions of 'shape' used in the measurements cited above, is beyond the scope of this paper. We emphasize, however, that the flattening in our stellar haloes cannot be attributed to any 'baryonic' effects such as a thin disc potential (e.g. Chiba & Beers 2001) or star formation in dissipative mergers and bulk gas flows (e.g. Bekki & Chiba 2001). Furthermore, it is unlikely to be the result of a (lesser) degree of flattening in the dark halo. Instead the structure of these components is most likely to reflect the intrinsically anisotropic distribution of satellite orbits. In certain cases (for example, Aq-D and Aq-A), it is clear that several contributing satellites with correlated trajectories are responsible for reinforcing the flattening of the inner halo.

4.2 Assembly history of the stellar halo

We now examine when and how our stellar haloes were assembled. Fig. 8 shows the mass fraction of each stellar halo (here *including* the accreted bulge component defined in Section 3.3) in place (i.e. unbound from its parent galaxy) at a given redshift. We count as belonging to the stellar halo all 'star particles' bound to the main dark halo and within 280 kpc of its centre at $z = 0$. This is compared with the growth of the corresponding host dark haloes. Our sample spans a range of assembly histories for haloes even though the halos have very similar final mass.

Not surprisingly, the growth of the dark halo is considerably more smooth than that of the stellar halo. The 'luminous' satellite accretion events contributing stars are a small subset of those that contribute to the dark halo, which additionally accretes a substantial fraction of its mass in the form of 'diffuse' dark matter (Wang et al. in prep.). As described in detail by Peñarrubia et al. (2008a,b), the dark haloes of infalling satellites must be heavily stripped before the deeply embedded stars are removed. This gives rise to time-lags
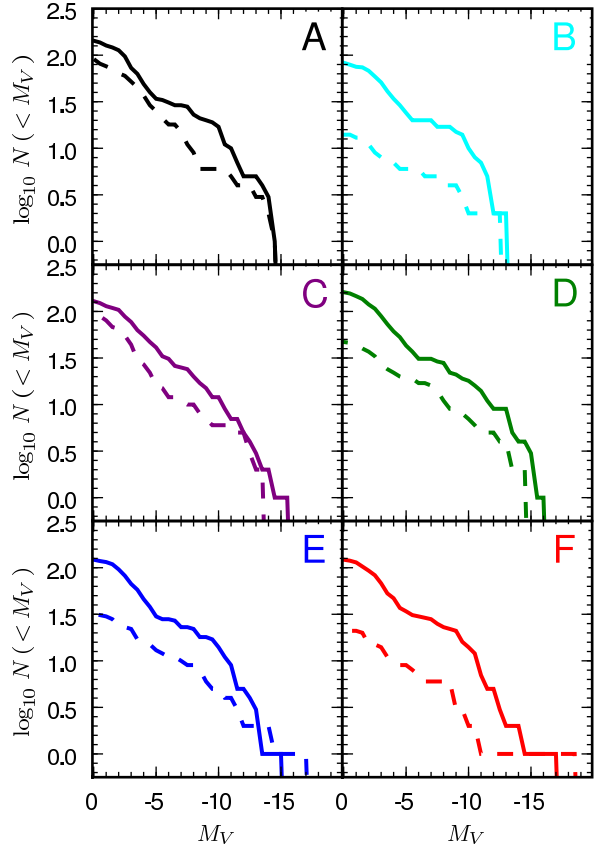

Figure 9. Luminosity functions of surviving satellites (solid) in each of our six haloes, compared with those of totally disrupted halo progenitors (dashed). These are constructed using only stars formed in each satellite before the time of infall (the halo-subhalo transition). The luminosity of each population is that after evolution to $z = 0$.

seen in Fig. 8 between the major events building dark and stellar haloes.

To characterise the similarities and differences between their histories, we subdivide our sample of six stellar haloes into two broad categories: those that grow through the gradual accretion of many progenitors (Aq-A, Aq-C and Aq-D) and those for which the majority of stellar mass is contributed by only one or two major events (Aq-B, Aq-E and Aq-F). We refer to this latter case as 'few-progenitor' growth. The measure of the number of 'most-significant' progenitors given in Table 2, N_{prog}, also ranks the haloes by the 'smoothness' of their accretion history, reflecting the intrinsically stochastic nature of their assembly.

Fig. 9 compares the luminosity functions (LFs) of surviving satellites with that of those totally disrupted to form the stellar halo, measuring luminosity at the time of infall in both cases. In general, there are fewer disrupted satellites than survivors over almost all luminosities, although the numbers and luminosities of the very brightest contributors and survivors are comparable in each halo. The deficit in the number of disrupted satellites relative to survivors is most pronounced in the few-progenitor haloes Aq-B and Aq-F.

Fig. 10 summarises the individual accretion events that contribute to the assembly of the stellar halo, plotting the stellar mass
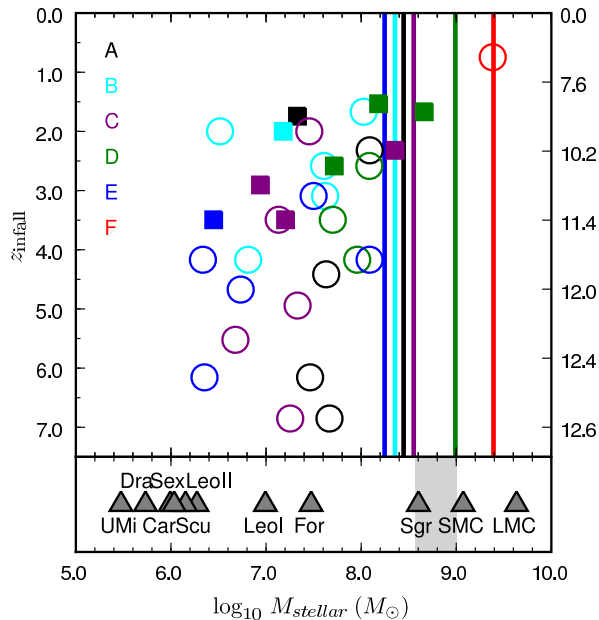
Figure 10. *Main panel*: for satellites that have been stripped to form the stellar haloes, symbols show the redshift of infall and total mass contributed to the stellar halo at $z = 0$ (in the range $3 < r < 280\,\mathrm{kpc}$). Vertical lines indicate the total mass of each stellar halo in this radial range. The right-hand y-axis is labelled by lookback time in gigayears. We plot only those satellites whose individual contributions, accumulated in rank order from the most significant contributor, account for 95% of the total stellar halo mass. Satellites totally disrupted by $z = 0$ are plotted as open circles, surviving satellites as filled squares (in almost all cases the contributions of these survivors are close to their total stellar masses; see text). *Lower panel:* symbols indicate the approximate masses of bright MW satellites, assuming a stellar mass-to-light ratio of 2; the Sgr present-day mass estimate is that given by Law, Johnston & Majewski (2005). The shaded region indicates an approximate range for the MW halo mass in our halo regime (see e.g. Bell et al. 2008).

Figure 11. Cumulative mass fraction of each stellar halo originating in satellites of stellar mass less than M_{sat}. Satellite masses are normalised to the total stellar halo mass M_{halo} in each case, as defined in Section 3.3.

of the most significant progenitor satellites against their redshift of infall (the time at which their host halo first becomes a subhalo of the main FOF group). Here we class as significant those satellites which together contribute 95% of the total halo stellar mass (this total is shown as a vertical line for each halo) when accumulated in rank order of their contribution. By this measure there are (5,6,8,6,6,1) significant progenitors for haloes (A,B,C,D,E,F). We also compare the masses of the brightest Milky Way satellites to the significant contributors in our stellar haloes. Typically the most significant contributors have masses comparable to the most massive surviving dwarf spheroidals, Fornax and Sagittarius.

With the exception of Aq-F, all the most significant contributors to our stellar haloes were accreted more than 8 Gyr ago. We highlight (as filled squares) those contributors whose cores survive as self-bound objects at $z = 0$. We find that surviving satellites accreted before $z = 1$ are the dominant contributors to the many-progenitor haloes Aq-C and Aq-D. The extreme case of Aq-F is atypical: more than 95% of the halo was contributed by the late merger of an object of stellar mass greater than the SMC infalling at $z \sim 0.7$, which does not survive. By contrast, the two least massive haloes Aq-B and Aq-E are built by many less massive accretions at higher redshift, with surviving satellites making only a minor contribution ($< 10\%$). Halo Aq-A represents an intermediate case, in which stars stripped from a relatively late-infalling survivor add
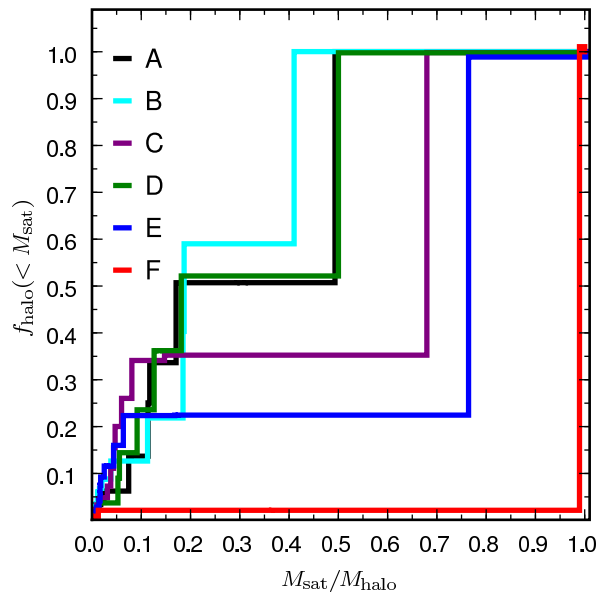
significantly ($\sim 10\%$) to the mass of a halo predominantly assembled at high redshift. The relative contributions to the halo of all accretion events are illustrated in Fig. 11. Each line in this figure indicates the fraction of the total halo stellar mass that was contributed by satellites donating less than a given fraction of this total *individually*. An interesting feature illustrated by this figure concerns Aq-B, one of our few-progenitor haloes (shown as light blue in all figures). Although Fig. 8 shows that the assembly of this halo proceeds over time by a series of concentrated 'jumps' in mass, its final composition is even less biased to the most significant progenitor than any of the many-progenitor haloes.

In general, surviving contributors to the halo retain less than 5% of the total stellar mass that formed in them. A small number of surviving contributors retain a significant fraction of their mass, for example, the surviving contributor to Aq-A, which retains 25%. In Fig. 12, we show histograms of the number of all surviving satellites (combining all six haloes) that have been stripped of a given fraction of their mass. Most satellites are either largely unaffected or almost totally stripped, indicating that the time spent in an intermediate disrupting state is relatively short.

In Table 2, we give the fraction of mass in the stellar halo that has been stripped from surviving satellites, f_{surv}. As previously stated, this contribution is dominant in haloes Aq-C (67%) and Aq-D (62%), significant in Aq-A (7%) and Aq-B (4%) and negligible in Aq-E and Aq-F. Sales et al. (2007b) find that only $\sim 6\%$ of stars in the eight haloes formed in the SPH simulations of Abadi et al. (2006) are associated with a surviving satellite. The lack of surviving satellites may be attributable to the limited resolution of those simulations; clearly, the number of 'survivors' is sensitive to the lowest mass at which remnant cores can be resolved. However, Bullock & Johnston (2005), and the companion study of Font et al. (2006), also conclude that the contribution of surviving satellites is small ($< 10\%$ in all of their 11 haloes and typically $< 1\%$). As the resolution of their simulations is comparable to ours, the predominance of surviving contributors in two of our haloes is significant.
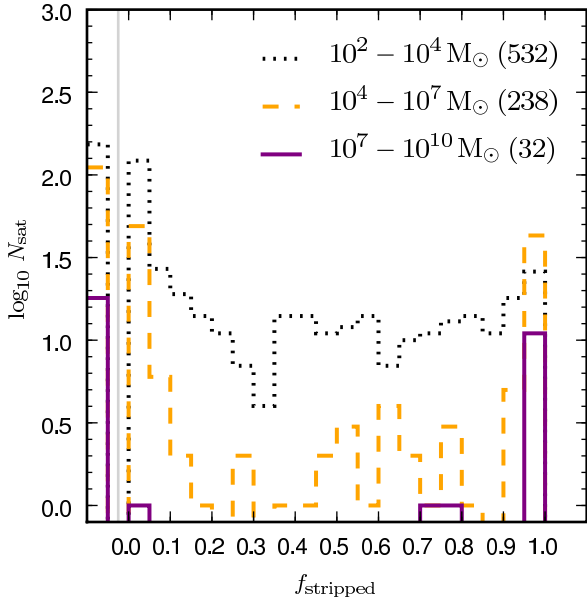
Figure 12. Number of surviving satellites (aggregated over all six haloes) which have lost a fraction, $f_{\rm stripped}$, of the stellar mass through tidal stripping. Satellites are divided into three mass bins: massive (purple), intermediate (dashed orange) and low-mass (dotted black) as quantified in the legend. The leftmost bin (demarcated by a vertical line) shows the number of satellites that have not suffered any stellar mass loss.

Bullock & Johnston find that their haloes are built from a similar (small) number of massive objects to ours (e.g. figure 10 of Bullock & Johnston 2005) with comparable accretion times (> 8 Gyr), suggesting that there are no fundamental differences in the infall times and masses of accreted satellites. Notably, Font et al. (2006) observe that no satellites accreted > 9 Gyr ago survive in their subsample of four of the Bullock & Johnston haloes, whereas we find that some satellites infalling even at redshifts $z > 2$ may survive (see also Fig. 16 below). The discrepancy appears to stem from the greater resilience of satellites accreted at $z > 1$ in our models, including some which contribute significantly to the stellar haloes. In other words, our model does not predict any more late-infalling contributors than the models of Bullock & Johnston. The more rapid disruption of massive subhaloes in the Bullock & Johnston models may be attributable to one or both of the analytic prescriptions employed by those authors to model the growth of the dark matter halo and dynamical friction in the absence of a live halo. It is also possible that the relation between halo mass and concentration assumed in the Bullock & Johnston model results in satellites that are less concentrated than subhaloes in the Aquarius simulations.

Current observational estimates (e.g. Bell et al. 2008) imply that the stellar halo of the Milky Way is intermediate in mass between our haloes Aq-C and Aq-D; if its accretion history is, in fact, qualitatively similar to these many-progenitor haloes, Fig. 10 implies that it is likely to have accreted its four or five most significant contributors around $z \sim 1 - 3$ in the form of objects with masses similar to the Fornax or Leo I dwarf spheroidals. Between one and three of the most recently accreted, and hence most massive contributors, are expected to retain a surviving core, and to have a stellar mass comparable to Sagittarius ($M_{\rm sgr} \sim 5 \times 10^8 \, {\rm M}_\odot$ or $\sim 50\%$

of the total[7] halo mass, infalling at a lookback time of $\sim 5 \, {\rm Gyr}$; Law et al. 2005). It is also possible that the Canis Major overdensity (with a core luminosity comparable to that of Sagittarius; Martin et al. 2004) associated with the low-latitude Monoceros stream (Newberg et al. 2002; Yanny et al. 2003; Ibata et al. 2003) should be included in the census of 'surviving contributors' (although this association is by no means certain; e.g. Mateu et al. 2009). Therefore, the picture so far established for the Milky Way appears to be in qualitative agreement with the presence of surviving cores from massive stellar halo contributors in our simulations.

4.3   Bulk halo properties and observables

4.3.1   Distribution of mass

In Fig. 13 we show the spherically averaged density profiles of halo stars (excluding material bound in surviving satellites, but making no distinction between streams, tidal tails or other overdensities, and a 'smooth' component). The notable degree of substructure in these profiles contrasts with the smooth dark matter haloes, which are well-fit by the Einasto profiles shown in Fig. 13. As discussed further below, this stellar substructure is due to the contribution of localised, spatially coherent subcomponents within the haloes, which are well resolved in our particle representation.

The shapes of the density profiles are broadly similar, showing a strong central concentration and an outer decline considerably steeper than that of the dark matter. We overplot in Fig. 13 an approximation of the Milky Way halo profile (Bell et al. 2008) and normalization (Fuchs & Jahreiß 1998; Gould et al. 1998). The gross structure of our three many-progenitor haloes Aq-A, Aq-C and Aq-D can be fit with broken power-law profiles having indices similar to the Milky Way ($n \sim -3$) interior to the break. Bell et al. (2008) note that their best-fitting observational profiles do not fully represent the complex structure of the halo, even though they mask out known overdensities (our fits include all halo substructure). Our fits decline somewhat more steeply than the Bell et al. data beyond their break radii. We suggest that the Milky Way fit may represent variation at the level of the fluctuations seen in our profiles, and that an even steeper decline may be observed with a representative and well-sampled tracer population to > 100 kpc (For example, Ivezić et al. 2000, find a sharp decline in counts of RR Lyr stars beyond ~ 60 kpc). In contrast with the many-progenitor haloes, two of our few-progenitor haloes (Aq-B and Aq-E) have consistently steeper profiles and show no obvious break. Their densities in the Solar shell are none the less comparable to the many-progenitor haloes. Aq-F is dominated by a single progenitor, the debris of which retains a high degree of unmixed structure at $z = 0$ (see also Fig. 15).

We show projected surface brightness profiles in Fig. 14. As with their three-dimensional counterparts, two characteristic shapes distinguish the many- and few-progenitor haloes. The few-progenitor haloes are centrally concentrated and well fit in their innermost ~ 10 kpc by Sersic profiles with $1.5 < n < 2.2$. Beyond 10 kpc, extended profiles with a more gradual rollover (described by Sersic profiles with $n \sim 1$ and $25 < r_{\rm eff} < 35$ kpc)

---

[7] Both the Sagittarius and Milky Way halo stellar mass estimates are highly uncertain; it is unclear what contribution is made by the Sgr debris to estimates of the halo mass, although both the stream and the Virgo overdensity were masked out in the analysis of Bell et al. (2008) for which a value of $\sim 3 \times 10^8 \, {\rm M}_\odot$ in the range $3 < r < 40$ kpc was obtained from a broken power-law fit to the remaining 'smooth' halo.
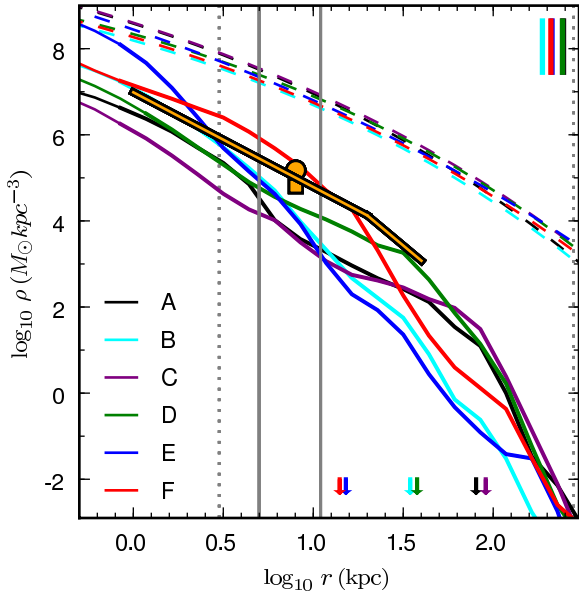
Figure 13. Spherically averaged density profiles for our six stellar haloes (shown as thin lines below the $\kappa = 7$ radius of Navarro et al. 2008, at which the circular velocity of the dark matter halo has converged to an accuracy of 1%). Arrows mark the break radii of broken power-law fits to each profile. Dashed lines show Einasto profile fits to the corresponding dark matter haloes (Navarro et al. 2008). Grey vertical lines demarcate our outer halo region (dotted) and the Solar neighbourhood (solid); coloured vertical bars indicate r_{200} for the dark haloes. For reference we overplot representative data for the Milky Way (orange): estimates of the halo density in the Solar neighbourhood (symbols) from Gould, Flynn & Bahcall (1998, square) and Fuchs & Jahreiß (1998, circle), and the best-fitting broken power-law of Bell et al. (excluding the Sagittarius stream and Virgo overdensity).

Figure 14. Radially averaged surface brightness profiles. Dashed lines show illustrative Sersic fits to haloes Aq-E and Aq-C (see text), with arrows indicating the corresponding scale radii. We show sections of equivalent profiles for the haloes of M31 (including the inner $r^{1/4}$ 'spheroid') and M33 (beyond 10 kpc) as dashed grey lines (Ibata et al. 2007). We overplot the surface number density (right-hand axis) of globular clusters in M31 (yellow squares) and the Milky Way (orange squares), with 40 and 10 clusters per bin, respectively. These profiles have been arbitrarily normalized to correspond to an estimate of the surface brightness of halo stars in the Solar neighbourhood from Morrison (1993), shown by a orange triangle. Vertical lines are as in Fig. 13

are a better fit to the many-progenitor haloes. In their centres, however, the many-progenitor haloes display a steep central inflection in surface brightness. As a consequence of these complex profiles, Sersic fits over the entire halo region (which we defined to begin at 3 kpc) are not fully representative in either case. To illustrate this broad dichotomy in Fig. 14, Sersic fits to a smoothly growing halo (Aq-C) *beyond* 10 kpc and a few-progenitor halo (Aq-E) *interior to* 10 kpc are shown. Abadi et al. (2006) found the average of their simulated stellar haloes to be well-fit by a Sersic profile ($n = 6.3$, $r_{eff} = 7.7$ kpc) in the radial range $30 < r < 130$ kpc, which we show as an orange dashed line in Fig. 14. This profile is close to the 'mean' profile of our halos A, C and D interior to 30 kpc (neglecting the significant fluctuations and inflections within each individual halo in Fig. 14), but does not capture the sharp decline of our haloes at radii beyond 150 kpc. Fig. 14 also shows (as dashed grey lines) the fits of Ibata et al. (2007) to the haloes of M31 (comprising an $r^{1/4}$ spheroid and shallow powerlaw tail at large radii) and M33 (powerlaw tail only).

There is evidence for multiple kinematic and chemical subdivisions within the Galactic globular cluster population (e.g. Searle & Zinn 1978; Frenk & White 1980; Zinn 1993; Mackey & Gilmore 2004, and refs. therein). This has led to suggestions that at least some of these cluster subsets may have originated in accreted satellites (Bellazzini, Ferraro & Ibata 2003; Mackey & Gilmore 2004; Forbes, Strader, & Brodie 2004). Support for this conclusion includes the presence of five globular clusters in the Fornax dwarf spheroidal (Hodge 1961) and the association of several Galac-
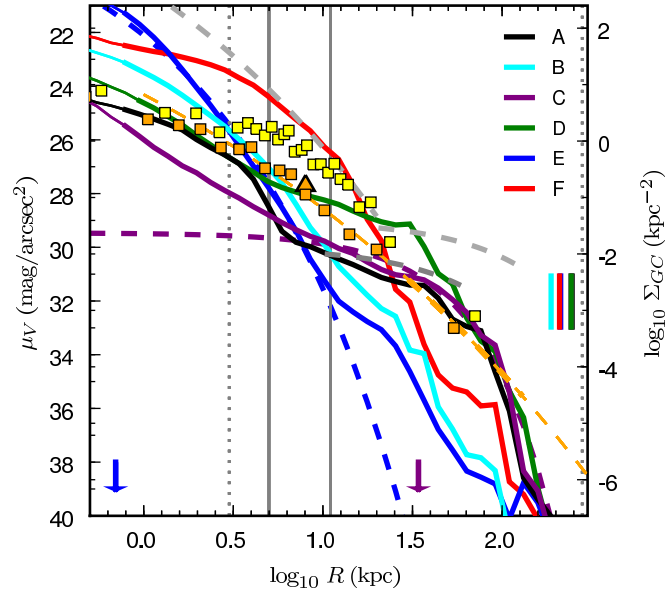
tic clusters with the Sagittarius nucleus and debris (e.g. Layden & Sarajedini 2000; Newberg et al. 2003; Bellazzini et al. 2003). Similarities with the 'structural' properties of stellar populations in the halo have motivated a longstanding interpretation of globular clusters as halo (i.e. accretion debris) tracers (e.g. Lynden-Bell & Lynden-Bell 1995). We therefore plot in Fig. 14 the surface density profile of globular clusters in the Milky Way (Harris 1996) and M31 (confirmed GCs in the Revised Bologna Catalogue – RBC v3.5, March 2008 Galleti et al. 2004, 2006, 2007; Kim et al. 2007; Huxor et al. 2008). The Milky Way data have been projected along an arbitrary axis, and the normalization has been chosen to match the surface density of Milky Way clusters to an estimate of the surface brightness of halo stars in the Solar neighbourhood ($\mu_V = 27.7$ mag/arcsec^2; Morrison 1993). We caution that the RBC incorporates data from ongoing surveys as it becomes available: the M31 GC profile shown here is therefore substantially incomplete, particularly with regard to the sky area covered beyond ~ 20–30 kpc.

Abadi et al. (2006) showed that their average stellar halo Sersic fit also approximates the distribution of globular clusters in the Milky Way and M31. As stated above, the inner regions of our haloes Aq-A, Aq-C and Aq-D are in broad agreement with the Abadi et al. halo profile, and hence show some similarities with the observed globular cluster profiles also. Both the halo and cluster samples show strong variations from halo to halo, however, and the comparison of these small samples is inconclusive. A close correspondence between accreted halo stars and globular clusters would be expected only if the majority of clusters are accreted, if accreted

satellites contribute a number of clusters proportionate to their stellar mass, and if all stripped clusters have an equal probability of surviving to $z = 0$. None of these assumptions is realistic, and further work is required better to constrain the relationship between globular clusters and stellar haloes.

The multicomponent nature of our haloes, which gives rise to the local structure in their overall profiles, is examined in more detail in Fig. 15. Here the density profiles of the major contributors shown in Fig. 10 are plotted individually (progenitors contributing $< 5\%$ of the halo have been added to the panel for Aq-F). It is clear from these profiles that material from a given progenitor can be deposited over a wide range of radii. The few-progenitor haloes show strong gradients in ρr^2 while more uniform distributions of this quantity are seen in their sub-dominant contributors and in most contributors to the many-progenitor haloes.

Finally, we show in Fig. 16 the time at which the satellite progenitors of halo stars at a given radius were accreted (this infall time is distinct from the time at which the stars themselves were stripped, which may be considerably later). An analogous infall time can be defined for the surviving satellites, which are shown as points in Fig. 16. We would expect little information to be encoded in an instantaneous sample of the radii of surviving satellites, but their infall times can none the less be usefully compared with those of halo stars.

A gradient to earlier infall times with decreasing radius is apparent in both the satellites and the many-progenitor haloes. In the case of the haloes, this reflects the fact that relatively larger apocentres are associated with later-infalling satellites, which enable them to deposit material over a greater radial range. Assembly in this manner is arguably not adequately characterised as 'inside out' formation; late infalling material is added at all radii but has a greater maximum extent than earlier-infalling material. The result is that earlier-infalling material comes to *dominate* towards the centre. For the few-progenitor haloes the profile of infall time is essentially flat (or shows sharp transitions between populations), more closely reflecting the contributions of individual progenitors.

Further to our discussion of satellite survival in our haloes in Section 4.2, it is interesting that amongst the surviving satellites, we observe several accreted at $z > 1$. For example, in the case of Aq-E, six surviving satellites are accreted at $z \sim 3.5$; at the present day this group is found in association with a concentration of halo stars from a stellar halo progenitor also infalling at this time. The majority of survivors in each halo are accreted recently, however, and typically more recently than the stellar halo progenitors. The opposite is true for the earliest-accreted survivors, which are accreted earlier than the halo at the notably small radii at which they are now found. In general, at any given instant the majority of satellites are more likely to be located nearer to the apocentre of their orbit than the pericentre; furthermore, the orbits of the most massive satellites are likely to have been more circular than their disrupted siblings and dynamical friction may act to reinforce such a trend. Therefore, the locations of early-infalling survivors are likely to be fairly represented by their radius in Fig. 16. Dynamical friction acts to contract but also to circularize orbits. Plausibly these survivors are those that have sunk slowly as the result of their initially low orbital eccentricities.

4.3.2 Stellar populations

In this section, we show how the multicomponent nature of our stellar haloes is reflected in their metallicity profiles, and contrast the stellar populations of surviving satellites with those of halo
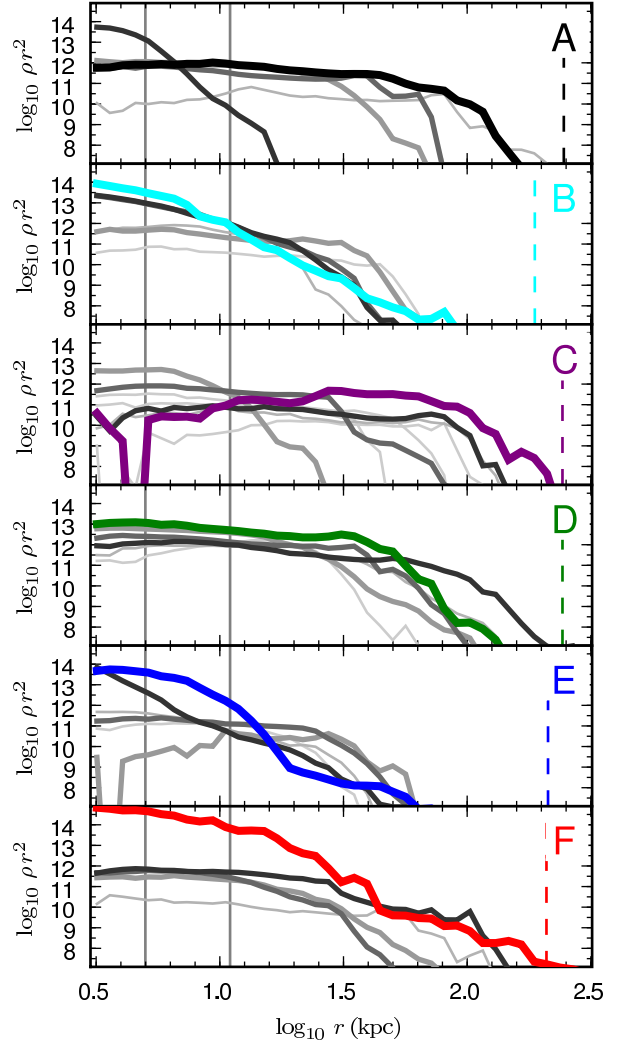

Figure 15. Individual density profiles (multiplied by r^2) for stars contributed by each of the most significant progenitors of the halo (defined in Section 3.3). Line types indicate the rank order of a progenitor contribution: the bold coloured line in each panel indicates the most significant contributor, while lesser contributions are shown by increasingly lighter and thinner lines. Vertical solid and dashed lines indicate the Solar shell and virial radius respectively, as Fig. 13. Individual stellar halo components contribute over a wide radial range, and different components 'dominate' at particular radii. This figure can be used to interpret the radial trends shown in other figures.

progenitors. We caution that a full comparison of the relationship between the stellar halo and surviving satellites will require more sophisticated modelling of the chemical enrichment process than is included in our fiducial model, which adopts the instantaneous recycling approximation and does not follow individual elemental abundances. We will address this detailed chemical modelling and related observational comparisons in a subsequent paper (De Lucia et al. in prep.). The model we adopt here tracks only total metallicity, defined as the total mass fraction of all metals relative to the Solar value, $Z/Z_\odot$ (the absolute value of which cannot be compared directly with measurements of [Fe/H]). This model can
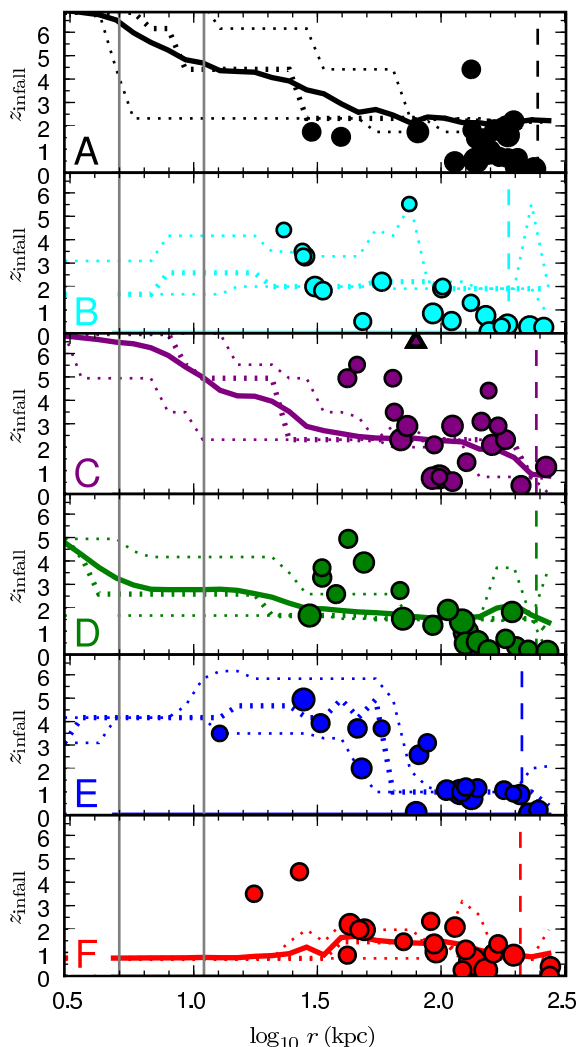
hibit global trends of outwardly declining metallicity gradients. In all cases the mean metallicity within the Solar radius is relatively high. These features can be explained by examining the relative weighting of contributions from individual progenitors at a given radius, as shown in the density profiles of Fig. 15, bearing in mind the mass-metallicity relation for satellites that arises in our model. Where massive progenitors make a significant luminosity-weighted contribution, the haloes are seen to be metal-rich. Overall, metallicity gradients are shallower in those haloes where many significant progenitors make a comparable contribution, smoothing the distribution over the extent of the halo. Conversely, metallicity gradients are steeper where only one or two disproportionately massive satellites make contributions to the halo (as indicated by the luminosity functions of Fig. 9). Sharp contrasts are created between the radii over which this metal-rich material is deposited (massive satellites suffer stronger dynamical friction and sink more rapidly, favouring their concentration at the centres of haloes) and a background of metal-poor material from less massive halo progenitors. This effect is clearly illustrated by the sharp transition in Aq-F and at two locations (centrally and at ~ 100 kpc) in Aq-E.

It follows that the process by which our smooth haloes are assembled, which gives rise to the steep gradients of progenitor infall time with redshift shown in Fig. 16, also acts to *erase* metallicity gradients. As a result, measurements of (for example) [Fe/H] alone do not constrain the local infall time; a metal-poor halo need not be 'old' in the sense of early assembly. A particularly notable example of this is Aq-E, where the centrally dominant metal-rich material was assembled into the halo considerably *earlier* ($z \sim 3$) than the diffuse outer envelope of relatively metal-poor material ($z \sim 1$). This is a manifestation of a mass-metallicity relation in satellites: at fixed luminosity, an earlier infall time is 'compensated' for by more rapid star formation, resulting in a comparable degree of overall enrichment as that for a satellite with similar luminosity infalling at lower redshift. Abundance ratios such as [α/Fe] indicate the time taken by a given stellar population to reach its observed level of enrichment, and so distinguish between rapidly forming massive populations, truncated by early accretion to the halo, and populations reaching similar mass and metallicity through gradual star formation (e.g. Shetrone, Côté & Sargent 2001; Tolstoy et al. 2003; Venn et al. 2004; Robertson et al. 2005).

Fig. 18 shows luminosity-weighted metallicity distribution functions (MDFs) for two selections of halo stars: a 'Solar shell' ($5 < r < 12$ kpc; dashed lines) and the entire halo as defined in Section 3.3 (dotted). We compare these to MDFs for stars in the surviving satellites in each halo, separating bright ($M_V < -10$, $r < 280$ kpc; thick, coloured) and 'faint' ($-10 < M_V < -5$; thin, grey) subsets. All distributions are normalized individually to the total luminosity in their sample of stars.

The MDF of Solar-shell halo stars is typically broad, and tends to peak at slightly higher metallicity (by < 0.5 dex) than the aggregated surviving bright satellites. The halo as a whole is comparable to the Solar shell. A clear disparity is only evident in Aq-E, where the halo appears to reflect more closely the distribution of fainter, lower-metallicity satellites. In all cases, the MDF of these faint satellites peaks at considerably lower metallicity than in the halo or brighter satellites. We find that the 'average' halo has an equivalent number of very metal-poor stars to the surviving bright satellites, although there are clear exceptions in individual cases. The fainter satellites have a substantially greater fraction of very metal-poor stars, in accordance with their low mean metallicities. Surviving satellites contain a greater fraction of moderately metal-poor stars ($\log_{10}(Z/Z_\odot) < -2.5$) than the halo.
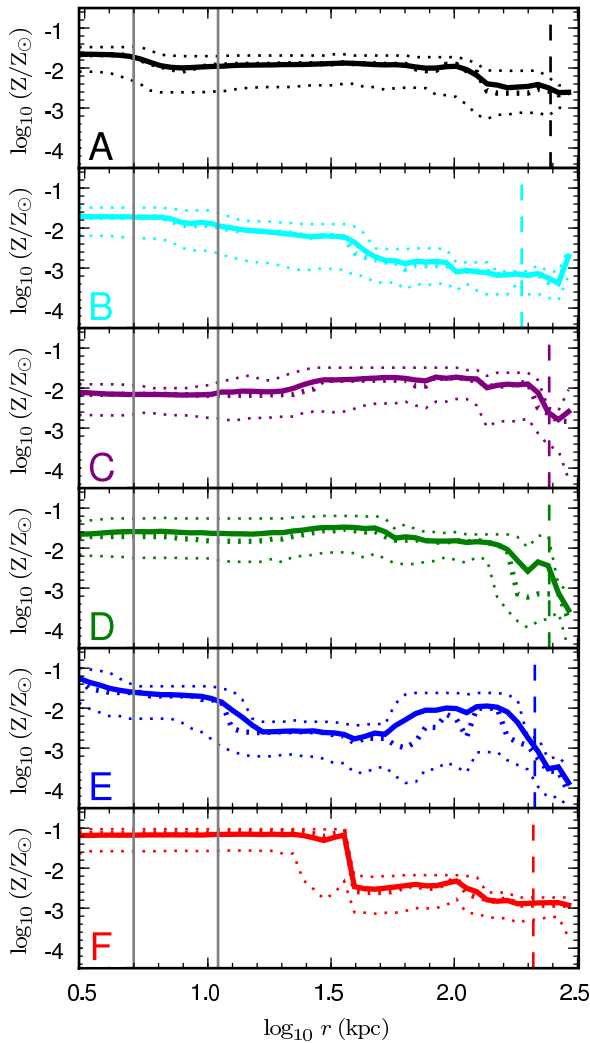

Figure 16. Lines show, for halo stars at a given radius at $z = 0$, the mean (solid), median and 10/90th percentile (dotted) redshift at which their parent galaxy was accreted on to the main halo (*not* the time at which the stars themselves were stripped). Filled circles show the redshift at which surviving satellites were accreted; triangles indicate satellites accreted before $z = 7$. Within the solar shell, the stellar halo is typically old in this 'dynamical' sense, whereas beyond 100 kpc its young 'dynamical' age is comparable to that of the surviving satellite population. In many cases the innermost satellites represent a relic population that is 'older' than the stellar halo at comparable radii.

nevertheless address the *relative* enrichment levels of different populations.

Fig. 17 shows the spherically averaged metallicity gradient in each halo. Our many-progenitor haloes are characterised by a metallicity distribution of width ~ 1 dex and approximately constant mean value, fluctuating by less than ± 0.5 dex over a range of 100 kpc. This is comparable to observations of the M31 halo, which show no significant gradient (metallicities varying by ± 0.14 dex) in the range 30–60 kpc (Richardson et al. 2009). Localised structure is most apparent in the few-progenitor haloes: Aq-F shows a clear separation into two components, while Aq-B and Aq-E ex-

Figure 17. Radial profiles of luminosity-weighted metallicity (ratio of total metal mass fraction to the Solar value) for spherical shells in our six haloes, showing the mean (solid) and median (thick dotted) profiles, bracketed by the 10th and 90th percentiles (dotted).
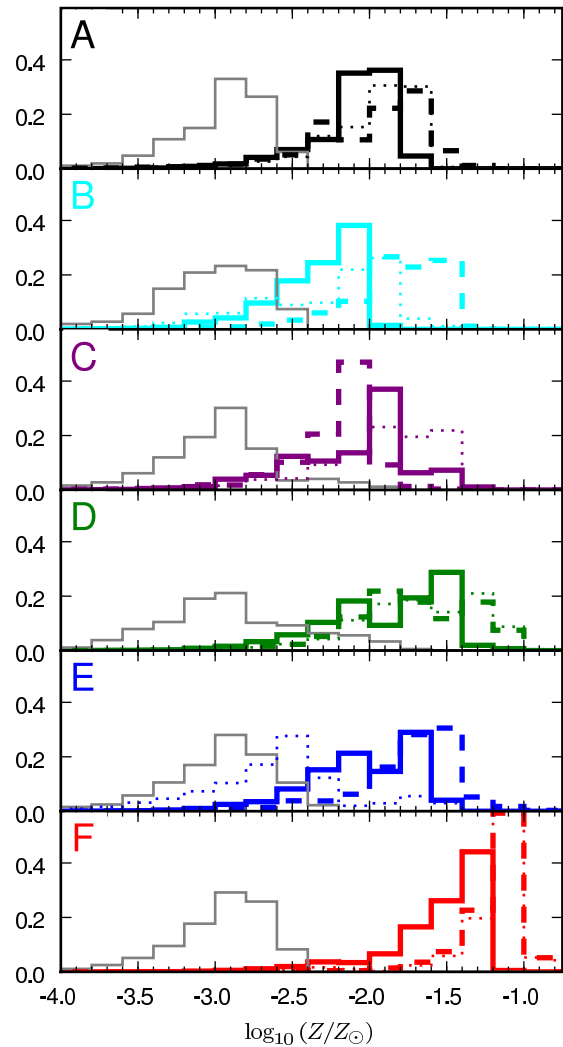
Figure 18. Metallicity distribution functions of bright ($M_V < -10$; solid coloured) and faint ($-10 < M_V < -5$; solid grey) satellites, halo stars in the 'Solar shell' (dashed) and the entire halo ($3 < r < 280$ kpc, dotted). Z is the total mass fraction of all metals.

Our halo models suggest that similar numbers of comparably luminous (and hence metal-rich) satellites contribute to the bright end of both the halo-progenitor and the surviving-satellite luminosity functions, and that these bright satellites are the dominant contributors to the halo. This supports the view that halo MDFs should resemble those of bright survivor satellites in their metal-poor tails. At very low metallicities the halo is dominated by the contribution of low-luminosity satellites which are exclusively metal-poor; the stars associated with these faint contributors are expected to represent only a very small fraction of the total halo luminosity.

Finally, Fig. 19 compares the luminosity-weighted age distributions of halo stars in the Solar shell with those in the surviving satellites ($M_V < -5$), separated into bright and faint subsets. The average of all six haloes contains essentially no stars younger than 5 Gyr (if we exclude halo Aq-F, which is strongly influenced by the late accretion of an SMC-like object, this minimum age rises to 8 Gyr). The median age of halo stars is ~ 11 Gyr. By contrast, the

brightest satellites have a median age of ~ 8 Gyr and a substantial tail to young ages (with $\sim 20\%$ younger than 4 Gyr and $\sim 90\%$ younger than the median halo age). The distribution of old stars in the faintest surviving satellites is similar to that of the halo.

The true age distribution of halo stars is poorly constrained in comparison to that of the satellites (e.g. Tolstoy, Hill & Tosi 2009). By comparing the colour and metallicity distributions of Milky Way halo stars to those of the Carina dSph, Unavane, Wyse & Gilmore (1996) have argued that similar satellites (i.e. those with a substantial fraction of intermediate-age stars) could not contribute more than $\sim 1\%$ to the halo (equivalent to a maximum of ~ 60 halo progenitors of Carina's luminosity). A corresponding limit of $\leqslant 6$ Fornax-like accretions in the last ~ 10 Gyr was derived from an analysis of higher metallicity stars by the same authors, consistent with the progenitor populations of our simulated stellar haloes.

It is important in this context that the satellites themselves form hierarchically. In our models, between ten and twenty pro-
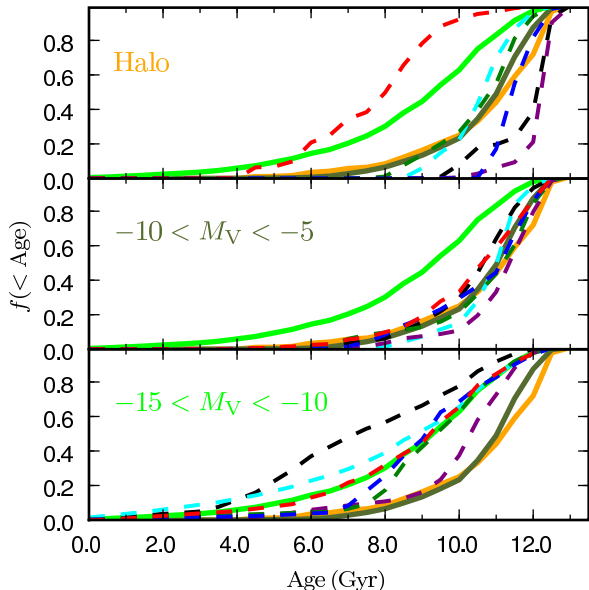
Figure 19. The cumulative luminosity-weighted age distribution (mean of all six simulations) for halo stars in the Solar shell ($5 < r < 12$ kpc, orange, top panel) compared to bright ($-15 < M_V < -10$; light green, bottom) and faint ($-10 < M_V < -5$; dark green, centre) satellites ($M_V < -10$), showing individual contributions from each halo (dashed, colours as in previous figures) to the mean value represented by each panel. The total stellar masses of these three components over all haloes are 1.04×10^9, 7.45×10^8 and 3.45×10^8 M$_\odot$, respectively.

genitors are typical for a (surviving) galaxy of stellar mass comparable to Sagittarius, or five to ten for a Fornax analogue. Satellites in this mass range are the most significant contributors to our stellar haloes. Their composite nature is likely to be reflected in their stellar population mix and physical structure, which could complicate attempts to understand the halo 'building blocks' and the surviving satellites in terms of simple relationships between mass, age and metallicity.

5   CONCLUSIONS

We have presented a technique for extracting information on the spatial and kinematic properties of galactic stellar haloes that combines a very high resolution fully cosmological ΛCDM simulation with a semi-analytic model of galaxy formation. We have applied this technique to six simulations of isolated dark matter haloes similar to or slightly less massive than that of the Milky Way, adopting a fiducial set of paramter values in the semi-analytic model GALFORM. The structural properties of the surviving satellites have been used as a constraint on the assignment of stellar populations to dark matter. We found that this technique results in satellite populations and stellar haloes in broad agreement with observations of the Milky Way and M31, if allowance is made for differences in dark halo mass.

Our method of assigning stellar populations to dark matter particles is, of course, a highly simplified approach to modelling star formation and stellar dynamics. The nature of star formation in dwarf galaxy haloes remains largely uncertain. In future, observations of satellites interpreted alongside high-resolution hydrodynamical simulations will test the validity of approaches such as

ours. As a further simplification, our models do not account for a likely additional contribution to the halo from scattered *in situ* (disc) stars, although we expect this contribution to be minimal far from the bulge and the disc plane. The results outlined here therefore address the history, structure and stellar populations of the accreted halo component in isolation.

Our results can be summarised as follows:

- Our six stellar haloes are predominantly built by satellite accretion events occurring between $1 < z < 3$. They span a range of assembly histories, from 'smooth' growth (with a number of roughly equally massive progenitors accreted steadily over a Hubble time) to growth in one or two discrete events.
- Stellar haloes in our model are typically built from fewer than 5 significant contributors. These significant objects have stellar masses comparable to the brightest classical dwarf spheroidals of the Milky Way; by contrast, fewer faint satellites contribute to the halo than are present in the surviving population.
- Typically, the most massive halo contributor is accreted at a lookback time of between 7 and 11 Gyr ($z \sim 1.5 - 3$) and deposits tidal debris over a wide radial range, dominating the contribution at large radii. Stars stripped from progenitors accreted at even earlier times usually dominate closer to the centre of the halo.
- A significant fraction of the stellar halo consists of stars stripped from individual *surviving* galaxies, contrary to expectations from previous studies (e.g. Bullock & Johnston 2005). It is the most recent (and significant) contributors that are likely to be identifiable as surviving bound cores. Such objects have typically lost $\sim 90\%$ of their original stellar mass.
- We find approximately power-law density profiles for the stellar haloes in the range $10 < r < 100$ kpc. Those haloes formed by a superposition of several comparably massive progenitors have slopes similar to those suggested for the Milky Way and M31 haloes, while those dominated by a disproportionally massive progenitor have steeper slopes.
- Our haloes have strongly prolate distributions of stellar mass in their inner regions ($c/a \sim 0.3$), with one exception, where an oblate, disc-like structure dominates the inner $10 - 20$ kpc.
- Haloes with several significant progenitors show little or no radial variation in their mean metallicity ($Z/Z_\odot$) up to 200 kpc. Those in which a small number of progenitors dominate show stronger metallicity gradients over their full extent or sharp transitions between regions of different metallicity. The centres of these haloes are typically more enriched than their outer regions.
- The stellar populations of the halo are likely to be chemically enriched to a level comparable to that of the bright surviving satellites, but to be as old as the more metal-poor surviving 'ultra faint' galaxies. The very metal-poor tail of the halo distribution is dominated by contributions from a plethora of faint galaxies that are insignificant contributors to the halo overall.

REFERENCES

Abadi M. G., Navarro J. F., Steinmetz M., 2006, MNRAS, 365, 747

Abadi M. G., Navarro J. F., Steinmetz M., Eke V. R., 2003, ApJ, 597, 21

Allgood B., Flores R. A., Primack J. R., Kravtsov A. V., Wechsler R. H., Faltenbacher A., Bullock J. S., 2006, MNRAS, 367, 1781

Baade W., 1944, ApJ, 100, 137

Barker M. K., Ferguson A. M. N., Irwin M., Arimoto N., Jablonka P., 2009, AJ, 138, 1469

Battaglia G., Helmi A., Morrison H., Harding P., Olszewski E. W., Mateo M., Freeman K. C., Norris J., et al., 2005, MNRAS, 364, 433

Baugh C. M., 2006, Reports on Progress in Physics, 69, 3101

Baugh C. M., Lacey C. G., Frenk C. S., Granato G. L., Silva L., Bressan A., Benson A. J., Cole S., 2005, MNRAS, 356, 1191

Bekki K., Chiba M., 2001, ApJ, 558, 666

Bell E. F., Zucker D. B., Belokurov V., Sharma S., Johnston K. V., Bullock J. S., Hogg D. W., Jahnke K., et al., 2008, ApJ, 680, 295

Bellazzini M., Ferraro F. R., Ibata R., 2003, AJ, 125, 188

Belokurov V., Evans N. W., Bell E. F., Irwin M. J., Hewett P. C., Koposov S., Rockosi C. M., Gilmore G., et al., 2007a, ApJ, 657, L89

Belokurov V., Evans N. W., Irwin M. J., Lynden-Bell D., Yanny B., Vidrih S., Gilmore G., Seabroke G., et al., 2007b, ApJ, 658, 337

Belokurov V., Zucker D. B., Evans N. W., Gilmore G., Vidrih S., Bramich D. M., Newberg H. J., Wyse R. F. G., et al., 2006, ApJ, 642, L137

Benson A. J., Bower R. G., Frenk C. S., Lacey C. G., Baugh C. M., Cole S., 2003, ApJ, 599, 38

Benson A. J., Frenk C. S., Lacey C. G., Baugh C. M., Cole S., 2002a, MNRAS, 333, 177

Benson A. J., Lacey C. G., Baugh C. M., Cole S., Frenk C. S., 2002b, MNRAS, 333, 156

Benson A. J., Lacey C. G., Frenk C. S., Baugh C. M., Cole S., 2004, MNRAS, 351, 1215

Bower R. G., Benson A. J., Malbon R., Helly J. C., Frenk C. S., Baugh C. M., Cole S., Lacey C. G., 2006, MNRAS, 370, 645

Boylan-Kolchin M., Springel V., White S. D. M., Jenkins A., Lemson G., 2009, MNRAS, 398, 1150

Brook C. B., Kawata D., Gibson B. K., Flynn C., 2004, MNRAS, 349, 52

Bullock J. S., Johnston K. V., 2005, ApJ, 635, 931

Busha M. T., Alvarez M. A., Wechsler R. H., Abel T., Strigari L. E., 2009, ArXiv e-prints, astro-ph/0901.3553

Carollo D., Beers T. C., Chiba M., Norris J. E., Freeman K. C., Lee Y. S., Ivezic Z., Rockosi C. M., et al., 2009, ArXiv e-prints, astro-ph/0909.3019

Carollo D., Beers T. C., Lee Y. S., Chiba M., Norris J. E., Wilhelm R., Sivarani T., Marsteller B., et al., 2007, Nature, 450, 1020

Chapman S. C., Ibata R., Irwin M., Koch A., Letarte B., Martin N., Collins M., Lewis G. F., et al., 2008, MNRAS, 390, 1437

Chiba M., Beers T. C., 2000, AJ, 119, 2843

—, 2001, ApJ, 549, 325

Cole S., Aragon-Salamanca A., Frenk C. S., Navarro J. F., Zepf S. E., 1994, MNRAS, 271, 781

Cole S., Lacey C. G., Baugh C. M., Frenk C. S., 2000, MNRAS, 319, 168

Croton D. J., Springel V., White S. D. M., De Lucia G., Frenk C. S., Gao L., Jenkins A., Kauffmann G., et al., 2006, MNRAS, 365, 11

de Jong R. S., Radburn-Smith D. J., Sick J. N., 2008, in Astronomical Society of the Pacific Conference Series, Vol. 396, Formation and Evolution of Galaxy Disks, Funes J. G., Corsini E. M., eds., p. 187

De Lucia G., Helmi A., 2008, MNRAS, 391, 14

De Lucia G., Springel V., White S. D. M., Croton D., Kauffmann G., 2006, MNRAS, 366, 499

Diemand J., Madau P., Moore B., 2005, MNRAS, 364, 367

Eggen O. J., Lynden-Bell D., Sandage A. R., 1962, ApJ, 136, 748

Faúndez-Abans M., Reshetnikov V. P., de Oliveira-Abans M., Fernandes I. F., 2009, Astronomy Letters, 35, 25

Ferguson A. M. N., Irwin M. J., Ibata R. A., Lewis G. F., Tanvir N. R., 2002, AJ, 124, 1452

Flynn C., Holmberg J., Portinari L., Fuchs B., Jahreiß H., 2006, MNRAS, 372, 1149

Font A. S., Bower R. G., McCarthy I. G., Benson A. J., Frenk C. S., Helly J. C., Lacey C. G., Baugh C. M., et al., 2008, MNRAS, 389, 1619

Font A. S., Johnston K. V., Bullock J. S., Robertson B. E., 2006, ApJ, 638, 585

Font A. S., Navarro J. F., Stadel J., Quinn T., 2001, ApJ, 563, L1

Forbes D. A., Strader J., Brodie J. P., 2004, AJ, 127, 3394

Freeman K., Bland-Hawthorn J., 2002, ARA&A, 40, 487

Frenk C. S., White S. D. M., 1980, MNRAS, 193, 295

Fuchs B., Jahreiß H., 1998, A&A, 329, 81

Galleti S., Bellazzini M., Federici L., Buzzoni A., Fusi Pecci F., 2007, A&A, 471, 127

Galleti S., Federici L., Bellazzini M., Buzzoni A., Fusi Pecci F., 2006, A&A, 456, 985

Galleti S., Federici L., Bellazzini M., Fusi Pecci F., Macrina S., 2004, A&A, 416, 917

Gilmore G., Reid N., 1983, MNRAS, 202, 1025

Gnedin N. Y., 2000, ApJ, 542, 535

Gould A., Flynn C., Bahcall J. N., 1998, ApJ, 503, 798

Grebel E. K., Gallagher I. I. I. . J. S., Harbeck D., 2003, AJ, 125, 1926

Guo Q., White S., Li C., Boylan-Kolchin M., 2009, ArXiv e-prints, astro-ph/0909.4305

Harris W. E., 1996, AJ, 112, 1487

Hatton S., Devriendt J. E. G., Ninin S., Bouchet F. R., Guiderdoni B., Vibert D., 2003, MNRAS, 343, 75

Helly J. C., Cole S., Frenk C. S., Baugh C. M., Benson A., Lacey C., 2003, MNRAS, 338, 903

Helmi A., 2008, A&A Rev., 15, 145

Helmi A., White S. D. M., 1999, MNRAS, 307, 495

Hodge P. W., 1961, AJ, 66, 83

Hoeft M., Yepes G., Gottlöber S., Springel V., 2006, MNRAS, 371, 401

Huxor A. P., Tanvir N. R., Ferguson A. M. N., Irwin M. J., Ibata R., Bridges T., Lewis G. F., 2008, MNRAS, 385, 1989

Ibata R., Chapman S., Ferguson A. M. N., Lewis G., Irwin M., Tanvir N., 2005, ApJ, 634, 287

Ibata R., Irwin M., Lewis G. F., Stolte A., 2001, ApJ, 547, L133

Ibata R., Martin N. F., Irwin M., Chapman S., Ferguson A. M. N., Lewis G. F., McConnachie A. W., 2007, ApJ, 671, 1591

Ibata R., Mouhcine M., Rejkuba M., 2009, MNRAS, 395, 126

Ibata R. A., Gilmore G., Irwin M. J., 1994, Nature, 370, 194

Ibata R. A., Irwin M. J., Lewis G. F., Ferguson A. M. N., Tanvir N., 2003, MNRAS, 340,

Irwin M., Hatzidimitriou D., 1995, MNRAS, 277, 1354

Ivezić v. Z., Goldston J., Finlator K., Knapp G. R., Yanny B., McKay T. A., Amrose S., Krisciunas K., et al., 2000, AJ, 120, 963

Johnston K. V., Hernquist L., Bolte M., 1996, ApJ, 465, 278

Jurić M., Ivezić v. Z., Brooks A., Lupton R. H., Schlegel D., Finkbeiner D., Padmanabhan N., Bond N., et al., 2008, ApJ, 673, 864

Kalirai J. S., Gilbert K. M., Guhathakurta P., Majewski S. R., Ostheimer J. C., Rich R. M., Cooper M. C., Reitzel D. B., et al., 2006, ApJ, 648, 389

Kang X., Jing Y. P., Mo H. J., Börner G., 2005, ApJ, 631, 21

Kauffmann G., Colberg J. M., Diaferio A., White S. D. M., 1999, MNRAS, 303, 188

Kauffmann G., Nusser A., Steinmetz M., 1997, MNRAS, 286, 795

Kazantzidis S., Bullock J. S., Zentner A. R., Kravtsov A. V., Moustakas L. A., 2008, ApJ, 688, 254

Kim S. C., Lee M. G., Geisler D., Sarajedini A., Park H. S., Hwang H. S., Harris W. E., Seguel J. C., et al., 2007, AJ, 134, 706

Kirby E. N., Simon J. D., Geha M., Guhathakurta P., Frebel A., 2008, ApJ, 685, L43

Komatsu E., Dunkley J., Nolta M. R., Bennett C. L., Gold B., Hinshaw G., Jarosik N., Larson D., et al., 2009, ApJS, 180, 330

Koposov S., Belokurov V., Evans N. W., Hewett P. C., Irwin M. J., Gilmore G., Zucker D. B., Rix H. W., et al., 2008, ApJ, 686, 279

Koposov S. E., Yoo J., Rix H. W., Weinberg D. H., Macciò A. V., Escudé J. M., 2009, ApJ, 696, 2179

Laird J. B., Carney B. W., Rupen M. P., Latham D. W., 1988, AJ, 96, 1908

Law D. R., Johnston K. V., Majewski S. R., 2005, ApJ, 619, 807

Layden A. C., Sarajedini A., 2000, AJ, 119, 1760

Li Y.-S., De Lucia G., Helmi A., 2009a, ArXiv e-prints, astro-ph/0909.1291

Li Y.-S., Helmi A., De Lucia G., Stoehr F., 2009b, MNRAS, 397,

Li Y.-S., White S. D. M., 2008, MNRAS, 384, 1459

Lynden-Bell D., Lynden-Bell R. M., 1995, MNRAS, 275, 429

Macciò A. V., Kang X., Moore B., 2009, ApJ, 692, L109

Mackey A. D., Gilmore G. F., 2004, MNRAS, 355, 504

Malin D., Hadley B., 1999, in Astronomical Society of the Pacific Conference Series, Vol. 182, Galaxy Dynamics - A Rutgers Symposium, D. R. Merritt M. Valluri . J. A. S., ed., p. 445

Martin N. F., de Jong J. T. A., Rix H. W., 2008, ApJ, 684, 1075

Martin N. F., Ibata R. A., Bellazzini M., Irwin M. J., Lewis G. F., Dehnen W., 2004, MNRAS, 348, 12

Martin N. F., McConnachie A. W., Irwin M., Widrow L. M., Ferguson A. M. N., Ibata R. A., Dubinski J., Babul A., et al., 2009, ArXiv e-prints, astro-ph/0909.0399

Martínez-Delgado D., Peñarrubia J., Gabany R. J., Trujillo I., Majewski S. R., Pohlen M., 2008, ApJ, 689, 184

Martínez-Delgado D., Pohlen M., Gabany R. J., Majewski S. R., Peñarrubia J., Palma C., 2009, ApJ, 692, 955

Mateo M. L., 1998, ARA&A, 36, 435

Mateu C., Vivas A. K., Zinn R., Miller L. R., Abad C., 2009, AJ, 137, 4412

McConnachie A. W., Chapman S. C., Ibata R. A., Ferguson A. M. N., Irwin M. J., Lewis G. F., Tanvir N. R., Martin N., 2006, ApJ, 647, L25

McConnachie A. W., Irwin M. J., Ibata R. A., Dubinski J., Widrow L. M., Martin N. F., Côté P., Dotter A. L., et al., 2009, Nature, 461, 66

Moore B., Diemand J., Madau P., Zemp M., Stadel J., 2006, MNRAS, 368, 563

Morrison H. L., 1993, AJ, 106, 578

Morrison H. L., Helmi A., Sun J., Liu P., Gu R., Norris J. E., Harding P., Kinman T. D., et al., 2009, ApJ, 694, 130

Morrison H. L., Mateo M., Olszewski E. W., Harding P., Dohm-Palmer R. C., Freeman K. C., Norris J. E., Morita M., 2000, AJ, 119, 2254

Navarro J. F., Ludlow A., Springel V., Wang J., Vogelsberger M., White S. D. M., Jenkins A., Frenk C. S., et al., 2008, ArXiv e-prints, astro-ph/0810.1522

Neto A. F., Gao L., Bett P., Cole S., Navarro J. F., Frenk C. S., White S. D. M., Springel V., et al., 2007, MNRAS, 381, 1450

Newberg H. J., Yanny B., Grebel E. K., Hennessy G., Ivezić v. Z., Martinez-Delgado D., Odenkirchen M., Rix H. W., et al., 2003, ApJ, 596, L191

Newberg H. J., Yanny B., Rockosi C., Grebel E. K., Rix H. W., Brinkmann J., Csabai I., Hennessy G., et al., 2002, ApJ, 569, 245

Okamoto T., Frenk C. S., 2009, MNRAS, 399, L174

Okamoto T., Frenk C. S., Jenkins A., Theuns T., 2009, ArXiv e-prints, astro-ph/0909.0265

Okamoto T., Gao L., Theuns T., 2008, MNRAS, 390, 920

Oort J. H., 1926, Publications of the Kapteyn Astronomical Laboratory Groningen, 40, 1

Peñarrubia J., McConnachie A., Babul A., 2006, ApJ, 650, L33

Peñarrubia J., McConnachie A. W., Navarro J. F., 2008a, ApJ, 672, 904

Peñarrubia J., Navarro J. F., McConnachie A. W., 2008b, ApJ, 673, 226

Peñarrubia J., Navarro J. F., McConnachie A. W., Martin N. F., 2009, ApJ, 698, 222

Power C., Navarro J. F., Jenkins A., Frenk C. S., White S. D. M., Springel V., Stadel J., Quinn T., 2003, MNRAS, 338, 14

Pritchet C. J., van den Bergh S., 1994, AJ, 107, 1730

Quinn P. J., 1984, ApJ, 279, 596

Quinn P. J., Hernquist L., Fullagar D. P., 1993, ApJ, 403, 74

Read J. I., Lake G., Agertz O., Debattista V. P., 2008, MNRAS, 389, 1041

Richardson J. C., Ferguson A. M. N., Mackey A. D., Irwin M. J., Chapman S. C., Huxor A., Ibata R. A., Lewis G. F., et al., 2009, MNRAS, 396, 1842

Robertson B., Bullock J. S., Font A. S., Johnston K. V., Hernquist L., 2005, ApJ, 632, 872

Sackett P. D., Morrisoni H. L., Harding P., Boroson T. A., 1994, Nature, 370, 441

Sales L. V., Navarro J. F., Abadi M. G., Steinmetz M., 2007a, MNRAS, 379, 1475

—, 2007b, MNRAS, 379, 1464

Schlaufman K. C., Rockosi C. M., Beers T. C., Bizyaev D., Brewington H., Lee Y. S., Malanushenko V., Malanushenko E., et al., 2009, ArXiv e-prints, astro-ph/0908.2627

Schweizer F., 1980, ApJ, 237, 303

Searle L., Zinn R., 1978, ApJ, 225, 357

Shang Z., Zheng Z., Brinks E., Chen J., Burstein D., Su H., Byun Y. I., Deng L., et al., 1998, ApJ, 504, L23

Shetrone M. D., Côté P., Sargent W. L. W., 2001, ApJ, 548, 592

Simon J. D., Geha M., 2007, ApJ, 670, 313

Smith M. C., Ruchti G. R., Helmi A., Wyse R. F. G., Fulbright J. P., Freeman K. C., Navarro J. F., Seabroke G. M., et al., 2007, MNRAS, 379, 755

Somerville R. S., 2002, ApJ, 572,

Spergel D. N., Verde L., Peiris H. V., Komatsu E., Nolta M. R., Bennett C. L., Halpern M., Hinshaw G., et al., 2003, ApJS, 148, 175

Springel V., 2005, MNRAS, 364, 1105

Springel V., Wang J., Vogelsberger M., Ludlow A., Jenkins A., Helmi A., Navarro J. F., Frenk C. S., et al., 2008a, MNRAS, 391, 1685

Springel V., White S. D. M., Frenk C. S., Navarro J. F., Jenkins A., Vogelsberger M., Wang J., Ludlow A., et al., 2008b, Nature, 456, 73

Springel V., White S. D. M., Jenkins A., Frenk C. S., Yoshida N., Gao L., Navarro J., Thacker R., et al., 2005, Nature, 435, 629

Springel V., White S. D. M., Tormen G., Kauffmann G., 2001, MNRAS, 328, 726

Starkenburg E., Helmi A., Morrison H. L., Harding P., van Woerden H., Mateo M., Olszewski E. W., Sivarani T., et al., 2009, ApJ, 698, 567

Strigari L. E., Bullock J. S., Kaplinghat M., Diemand J., Kuhlen M., Madau P., 2007, ApJ, 669, 676

Strigari L. E., Bullock J. S., Kaplinghat M., Simon J. D., Geha M., Willman B., Walker M. G., 2008, Nature, 454, 1096

Tanaka M., Chiba M., Komiyama Y., Guhathakurta P., Kalirai J. S., Iye M., 2009, ArXiv e-prints, astro-ph/0908.0245

Tollerud E. J., Bullock J. S., Strigari L. E., Willman B., 2008, ApJ, 688, 277

Tolstoy E., Hill V., Tosi M., 2009, ArXiv e-prints, astro-ph/0904.4505

Tolstoy E., Venn K. A., Shetrone M., Primas F., Hill V., Kaufer A., Szeifert T., 2003, AJ, 125, 707

Toth G., Ostriker J. P., 1992, ApJ, 389, 5

Tremonti C. A., Heckman T. M., Kauffmann G., Brinchmann J., Charlot S., White S. D. M., Seibert M., Peng E. W., et al., 2004, ApJ, 613, 898

Unavane M., Wyse R. F. G., Gilmore G., 1996, MNRAS, 278, 727

Velazquez H., White S. D. M., 1999, MNRAS, 304, 254

Venn K. A., Irwin M., Shetrone M. D., Tout C. A., Hill V., Tolstoy E., 2004, AJ, 128, 1177

Vivas A. K., Zinn R., 2006, AJ, 132, 714

Walker M. G., Mateo M., Olszewski E. W., Peñarrubia J., Wyn Evans N., Gilmore G., 2009, ArXiv e-prints, astro-ph/0906.0341

Watkins L. L., Evans N. W., Belokurov V., Smith M. C., Hewett P. C., Bramich D. M., Gilmore G. F., Irwin M. J., et al., 2009, MNRAS, 398, 1757

White S. D. M., Springel V., 2000, in The First Stars, Weiss A., Abel T. G., Hill V., eds., p. 327

Wolf J., Martinez G. D., Bullock J. S., Kaplinghat M., Geha M., Munoz R. R., Simon J. D., Avedo F. F., 2009, ArXiv e-prints, astro-ph/0908.2995

Xue X. X., Rix H. W., Zhao G., Re Fiorentin P., Naab T., Steinmetz M., van den Bosch F. C., Beers T. C., et al., 2008, ApJ, 684, 1143

Yanny B., Newberg H. J., Grebel E. K., Kent S., Odenkirchen M., Rockosi C. M., Schlegel D., Subbarao M., et al., 2003, ApJ, 588, 824

Yanny B., Newberg H. J., Kent S., Laurent-Muehleisen S. A., Pier J. R., Richards G. T., Stoughton C., Anderson Jr. . J. E., et al., 2000, ApJ, 540, 825

Yanny B., Rockosi C., Newberg H. J., Knapp G. R., Adelman-McCarthy J. K., Alcorn B., Allam S., Allende Prieto C., et al., 2009, AJ, 137, 4377

Yoachim P., Dalcanton J. J., 2005, ApJ, 624, 701

—, 2008, ApJ, 682, 1004

Zibetti S., Ferguson A. M. N., 2004, MNRAS, 352,

Zibetti S., White S. D. M., Brinkmann J., 2004, MNRAS, 347, 556

Zinn R., 1993, in The Globular Cluster-Galaxy Connection, Smith G. H., Brodie J. P., eds., Vol. 48, p. 38

Zolotov A., Willman B., Brooks A. M., Governato F., Brook C. B., Hogg D. W., Quinn T., Stinson G., 2009, ApJ, 702, 1058

This paper has been typeset from a TEX/ LATEX file prepared by the author.